The neurogenic fate of the hindbrain boundaries: a Notch-dependent behavioral switch triggers asymmetric division of boundary stem cells

Covadonga F Hevia[1], Carolyn Engel-Pizcueta[1], Frederic Udina[2,3], and Cristina Pujades[1]

[1]Department of Experimental and Health Sciences, [2]Department of Economics and Business, Universitat Pompeu Fabra, [3]Data Science Center, Barcelona Graduate School of Economics, Barcelona, Spain

*Correspondence to:
Cristina Pujades, PhD
Department of Experimental and Health Sciences
Universitat Pompeu Fabra
PRBB, Dr Aiguader 88, 08003 Barcelona, SPAIN
cristina.pujades@upf.edu
ORCID ID CP: 0000-0001-6423-7451

SHORT TITLE: Neurogenic fate of hindbrain boundaries

KEYWORDS: neurogenesis, asymmetric divisions, neural progenitors, tissue segmentation, boundaries, morphogenesis, hindbrain, Notch-signalling, stem cells

SUMMARY

The generation of cell diversity in the central nervous system occurs during embryogenesis and requires a precise balance between stem cell proliferation, neuronal commitment to specific fates, and further differentiation. Understanding the cellular and molecular mechanisms regulating this balance in the embryonic brain is challenging. Here we reveal how the neurogenic capacity in the hindbrain is differently allocated to distinct domains over time, and how the boundary cells undergo a functional transition to become neurogenic during zebrafish hindbrain segmentation. By generating a CRISPR-based knock-in transgenic line to specifically label the boundary cell population, we tracked their derivatives over time and followed their behavior, allowing us to identify how asymmetric cell divisions arise and to reconstruct the trajectories of the boundary derivatives through the progenitor and differentiated domains. The behavioral switch in boundary cells is triggered by the onset of Notch signaling, based on lateral inhibition at the dorsoventral level. Our findings reveal that distinct neurogenic phases take place during hindbrain growth and suggest that boundary cells contribute to refine the final number, identity, and proportion of neurons in the brain.

INTRODUCTION

In the central nervous system, the assembly of functional neural circuits requires both the specification of neuronal identities and the execution of genetic developmental programs that establish precise neural network wiring. During embryonic development, neural stem cells must balance self-renewal, commitment to specific fates and differentiation, to generate the wide diversity of neurons in the correct numbers and proportions. How spatiotemporally controlled cell proliferation, specification, and differentiation occur alongside morphogenesis to construct a functional brain is still poorly understood. Addressing this has been technically challenging to date; no *in vitro* system can recapitulate this *in vivo* process, which involves an extraordinary well-orchestrated migration of differentiated neurons from their birth site as well as complex tissue morphogenetic movements over time. Thus, reconstructing cell lineages is central to understanding how the wide diversity of cell types is generated. Recent developments in 4D imaging (e.g., 3D plus time) and cell-tracking tools now permit simultaneous measurements at high spatiotemporal coverage and resolution, allowing the assessment of cell lineages and cell behavior in the whole organ context (Dyballa et al., 2017; McDole et al., 2018; Wan et al., 2019; Wolff et al., 2018).

Cell diversity is generated during embryogenesis at the same time that the brain undergoes a dramatic transformation from a simple tubular structure —the neural tube— to a highly convoluted structure —the brain, resulting in changes in the position of neuronal progenitors and their derivatives over time. Generation of neuronal heterogeneity requires tight coordination between the maintenance of neural stem cells, the acquisition of neurogenic capacity, and the changes in the relative spatial distribution of both progenitors and derivatives during morphogenesis. In this light, the Notch pathway is of interest, as it is key regulator of neurogenesis in several contexts and can single-out cells from equipotent progenitor fields through the lateral inhibition mechanism (Louvi and Artavanis-Tsakonas, 2006). However, how Notch signalling operates in coordination with the complex brain morphogenetic movements is still unclear.

The hindbrain is an interesting structure to take on this challenge, since it constitutes the embryonic brainstem, which controls life-sustaining functions and is extremely conserved in vertebrates. The hindbrain undergoes a dynamic self-organization, which involves the segmentation of the tissue leading to the transitory formation of seven metameres named rhombomeres (r). Rhombomeres constitute developmental units of gene expression and cell lineage compartments (Fraser et al., 1990; Jimenez-Guri et al., 2010; Kiecker and Lumsden, 2005). They are separated by cellular interfaces called hindbrain boundaries (Guthrie and Lumsden, 1991), which exhibit specific gene expression (Cheng et al., 2004; Letelier et al., 2018). Cells within these boundaries display distinct functions as development proceeds (for review see Pujades, 2020). First, they act as morphomechanical barriers to prevent cell intermingling between adjacent rhombomeres (Calzolari et al., 2014). When rhombomeric lineages are segregated, they constitute a signaling hub that instructs the differentiation and organization of neurons in the neighboring rhombomeres (Cooke et al., 2005; Riley et al., 2004; Terriente et al., 2012). Concomitantly, boundary cells behave as a pool of progenitors, maintaining neural stem cells in an active proliferative state through Yap/Taz-TEAD activity (Voltes et al., 2019). While rhombomeric regions are actively engaged in neurogenesis, hindbrain boundaries are devoid of proneural genes, acting as non-neurogenic territories (Nikolaou et al., 2009); however, recent evidence suggests that boundaries provide differentiating neurons to the hindbrain (Peretz et al., 2016; Voltes et al., 2019). Several questions remain unclear, however, such as how stemness vs. differentiation is balanced, the fate of the boundary cells, and what is the cell lineage and identity of the neurons derived from the boundaries.

Here, we have addressed these questions by specifically studying the transition from stem cells towards cell differentiation, and by following the fate of the whole boundary cell population in the hindbrain of zebrafish. We have generated a versatile CRISPR-based knock-in zebrafish transgenic line that specifically targets the boundary cell population. We found that boundary cells undergo a switch in their behavior, triggered by Notch-signaling, which seems to operate through lateral inhibition along the dorsoventral axis. By reconstructing the lineage of boundary cells, we unveiled that boundary cells transition from neuroepithelial stem cells to radial glia cells that undergo asymmetric divisions. Thus, boundaries constitute a self-renewing pool of

stem cells and provide neurons to the hindbrain, although this neurogenic capacity is delayed in respect to the adjacent rhombomeric territories. Eventually, boundary cells undergo differentiation, thus contributing to refine the number, identity, and proportion of neurons in the brain.

RESULTS

Neuron differentiation in the hindbrain boundaries is delayed with respect to the rhombomeric territories

Our previous studies showed that boundary cells undergo neurogenesis when Yap/Taz-TEAD activity ended (Voltes et al., 2019). However, the cell lineage, the timing of neurogenesis, and their final neuron identity remain unknown. Here, we deeply studied how proliferating progenitors transition to differentiated neurons in the zebrafish hindbrain. First, immunostaining the hindbrain tissue with the neural progenitor cell marker Sox2 and the pan-neuronal differentiation marker HuC revealed that the neuronal differentiation domain in the overall hindbrain dramatically increased over time at the expense of the progenitor domain, which concomitantly diminished (Figure 1A–1C). At 24 hours-post-fertilization (hpf), which is at early stages of embryonic development when neuronal differentiation in the hindbrain has just started, differentiated neurons were mainly allocated to the mantle zone of the rhombomeric regions (Figure 1A; see transverse view in (a)). In contrast, boundary regions did not harbor differentiated neurons at this early time point (Figure 1A; see transverse view in (a')). Nevertheless, this changed by 32 hpf, at which point differentiated neurons appeared in boundary regions (Figure 1B; compare b-b'). By 48 hpf, there were almost no differences between the mantle zone of boundaries and neighboring rhombomeric territories (Figure 1C; compare c-c'), with both allocating many differentiated neurons. Thus, the growth of the neuronal differentiation domain in the hindbrain boundaries occurred mainly between 32 and 48 hpf, indicating a clear delay as compared to the neighboring rhombomeres. However, it could not be discerned if the differentiated neuronal pool residing in the boundaries arose exclusively from boundary progenitor cells or from the highly neurogenic neighboring regions.

To unveil the specific contribution of hindbrain boundary cells to the overall neuronal differentiation domain, we built up a highly versatile zebrafish transgenic line that specifically labels the boundary cell population (BCP). Our strategy was based in knocking-in the *Gal4* gene, into one of the *cis*-regulatory elements responsible for driving gene expression to the hindbrain boundary cells (Letelier et al., 2018). We

targeted a genomic position located upstream of the transcriptional start site (TSS) of the *sgca* locus (Kimura et al., 2014) (Figures 1D, S1A, and S1B); note that a target site was designed at about 90 base pairs (bp) upstream of the ATG start codon of *sgca*. Several transgenic lines were generated by combining the Gal4 knock-in line with different UAS reporters (Figure S1C), and efficient expression was driven to the hindbrain boundary cells (Figure 1E), as confirmed using the Tg[elA:GFP] line as a landmark for rhombomeres 3 and 5 (Figure 1F).

We used the Tg[BCP:H2AmCherry] fish line, which expressed mCherry in the boundary cells nuclei, to study how spatiotemporally coordinated cell progenitor specification and differentiation occurred in the hindbrain boundaries alongside morphogenesis. First, we characterized this transgenic line by comparing the onset of *sgca* expression with the onset of *mCherry*. As expected, there was a short delay between the expression of the two genes: whereas *sgca* onset was before 20 hpf (Letelier et al., 2018; Figures S2A-S2B), *mCherry* was partially expressed in the boundaries at 20 hpf (Figure S2A', S2B), while all boundary cells expressed *sgca* and *mCherry* only at 24 hpf (Figures S2C and S2D). Both *sgca* and *mCherry* expression in the boundary cells remained at least until 30 hpf (Figure S2E), as was also observed with other boundary markers such as *rfng* (Figures S2G-S2L). We consistently detected mCherry protein in the boundaries around 24 hpf (Figure 1G; see transverse views in (g)) and, by 30 hpf, most of the boundary progenitor cells displayed *mCherry* (Figure 1H; see transverse views in (h)). Interestingly, during this temporal window, we clearly observed how boundary neural progenitors dramatically changed their position due to hindbrain morphogenesis, such that all progenitor cells became dorsally positioned (Figure 1h and 1i; note that the ventricular surface occupied all the dorsal part of the hindbrain). The stability of the mCherry protein extended beyond the interval of expression of the classical boundary markers, such as *rfng* or *sgca* (compare Figure 1I with Figures S2M and S2N) (Letelier et al., 2018). This made using this transgenic line advantageous for following the fate of these progenitor cells even at later stages, in which boundary markers were no longer expressed. Accordingly, we observed mCherry-expressing cells in the neuronal differentiation domain at 48 hpf (Figures 1I and S2R), indicating that (as previously reported) boundary cells can undergo neurogenesis (Peretz et al., 2016; Voltes et al., 2019). These results also indicated that neuronal differentiation in the

boundaries did not occur at the same time than in their neighboring rhombomeric cells. As expected, the mCherry boundary cells displayed Yap/Taz-TEAD activity (Figures S2O–S2R; Voltes et al., 2019). Furthermore, the Tg[BCP:H2AmCherry] fish line was specific for boundary cells not fated to the rhombic lip, which is a transient neuroepithelial structure that expands all along the dorsolateral hindbrain and expresses the proneural gene *atoh1a* (Figures 1J and 1K). Thus, the newly generated and versatile Tg[BCP:reporter] lines are excellent tools to study in-depth the *in vivo* behavior of the hindbrain boundary cell populations over time.

Boundary cells undergo a Notch-dependent functional switch

To confirm that boundary cells were delayed in undergoing neurogenesis as compared to the neighboring territories, we generated double transgenic embryos Tg[BCP:H2AmCherry;HuC:GFP] and assessed the position of boundary cells and their derivatives *in vivo*, in both the progenitor and the differentiation domains, at distinct embryonic stages, and determined whether they expressed HuC. At 30 hpf, almost all mCherry-expressing cells remained in the ventricular domain and did not express the differentiation marker HuC (Figure 2A; see transverse view in (a)). This indicated that boundary cells were maintained as neural stem cells, and that differentiated neurons residing in the mantle zone of the boundaries at 30 hpf most probably arose from adjacent territories. However, when we performed the same analysis at 48 hpf, an average of 42% of cells expressing mCherry —e.g., derived from the boundary progenitor cell population— were in the neuronal differentiation domain and expressed HuC (Figure 2B, see inserts; transverse view in (b)). This resulted in an increase of differentiated neurons originated from the boundary progenitors during this morphogenetic period; for instance, the r5/r6 boundary had 1.6% of progenitors [1.6/99 cells] at 30 hpf vs. 40.10% [79/197 cells] at 48 hpf (Figure 2C; Table 1).

Previous studies showed the role of *Lfng* in the regulation of neurogenesis in the rhombomeres at early embryonic stages through Notch signaling, with no effects on the hindbrain boundaries (Nikolaou et al., 2009). Thus, we wanted to evaluate whether Notch-activity was involved in the change in behavior of boundary cells —progenitor vs. differentiated cells— at this later developmental stage. For this, we first assessed

Notch-activity in the hindbrain using the Tg[tp1:d2GFP] transgenic line, which is a readout of Notch-active cells (Clark et al., 2012). As expected, we observed that boundary cells were devoid of Notch-activity at early stages (Figure 2D, and inserts; see mCherry cells with no GFP expression in (d)). In contrast, the rhombic lip and the rhombomeric territories were Notch-active (Figures 2D and S3A; Belzunce et al., 2020). However, by 48 hpf, most of the boundary progenitor cells were Notch-active (Figure 2E, and inserts; see in (e) transverse views and corresponding inserts, showing that most of the dorsal mCherry cells facing the ventricle expressed GFP). This dramatic increase in Notch-activity was already evident from 26 hpf to 36 hpf, as the percentage of boundary progenitor cells displaying Notch activity increased from 6.4% [2.6/40 cells] to 64% [73/114 cells] as example of the r5/r6 boundary (Figure 2F; Tables 2A and 2B). The detailed analysis of the Notch-active boundary cells allowed us to appreciate their morphology (thanks to the GFP associated to the Notch reporter), which revealed that the radial glia cells had the soma facing the ventricle and the radial projections towards the basal part (Figure S4A). Accordingly, these cells were positively immunostained with the zrf1 antibody (Figure S4B), a marker of radial glia processes (Trevarrow et al., 1990). Overall, these observations suggest that Notch signaling is responsible for transitioning boundary neuroepithelial progenitors to radial glia cells, thus triggering neurogenesis in the boundaries.

We next conditionally inhibited Notch activity by incubating Tg[BCP:H2AmCherry;HuC:GFP] embryos with the gamma-secretase inhibitor LY411575 at different time intervals, and checked for effects of this on neuronal differentiation (Figure 2G). First, we inhibited Notch when only rhombomeric regions are highly engaged in neurogenesis (20–26 hpf). As expected, the size of the HuC domain dramatically increased, although none of the mCherry-positive cells expressed HuC (Figures 2H and 2I). In contrast, when Notch-activity was inhibited at the period in which boundary cells started to be engaged in neurogenesis (30–36 hpf), boundary cells massively differentiated and expressed HuC (Figures 2J and 2K

w). These results demonstrate that Notch-activity triggers the transition of boundary progenitor cells towards differentiation.

Next, we wanted to investigate the main Notch-players in this cell population and whether their expression changed upon the switch in cell behavior. When boundary cells were not undergoing neurogenesis (26 hpf), we observed a faint expression of *notch3* receptor in the whole hindbrain (Figure 3A, see transverse view in (a); Figure S3B). Indeed, the expression of *notch3* receptor in the hindbrain seemed to start later than other *notch* receptors such as *notch1a,* which is already highly expressed in rhombomeric cells at 18 hpf, but excluded from the boundary cells (Nikolaou et al., 2009). Boundaries were mainly devoid of *deltaD* ligand at 26 hpf (Figure 3A', see transverse view in (a') and inserts), although, as expected, rhombomeres expressed *deltaD* (Figure S3C; Cheng et al., 2004). By 36 hpf, when approximately 64% of the boundary cells were Notch-active, all cells located at the ventricular zone displayed *notch3* (Figure 3B, see transverse view in (b, b''); Figure S3E). Boundary cells also started to express *deltaD* (Figure 3B', b', b'''). As expected, *deltaD* and *notch3* expression did not overlap (Figure 3B-B', see transverse (b'''') and inserts). Interestingly, cells expressing *notch3* were always in the most ventricular domain (Figure 3b, b'', b''''), whereas *deltaD*-cells were just underneath *notch3*-cells (Figure 3b', b''', b''''). The same dorsoventral spatial pattern was appreciated in rhombomeric regions at this stage (Figures S3B and S3C, S3E-G). This supports the previous observation that Notch-activity was restricted to the most ventricular cells, both in the boundaries and in the rhombomeres (Figure 2E, see transverse view in (e); Figure S3D). The fact that the increase of *notch3* expression correlated with the triggering of Notch-activity in the boundary cells, and that the expression of *notch3* was more homogenous in the most dorsal cell layer than *notch1a* (Figures S3H and S3I), suggested that Notch3 and DeltaD could be relevant players in the boundary cells. We then checked for the expression of the proneural genes *ascl1b* and *neuroD4* as downstream targets of Notch-signaling. At 26 hpf, these genes were not expressed in boundary cell progenitors but were expressed in the adjacent territories (Figure 3C-C', c-c'''') (Nikolaou et al., 2009). However, when boundary cells were engaged in neurogenesis (at 36 hpf), their derivatives expressed *ascl1b* and *neuroD4* and, accordingly, were located in a more basal domain (Figure 3D-D', d''-d''''). This demonstrates that boundary cells are competent for undergoing neuronal differentiation and suggests that the Notch canonical mechanism of lateral inhibition

operates along the dorsoventral axis.

Following the behavior of boundary cells upon hindbrain morphogenesis

To produce a hindbrain of a specified robust size and composition, the rates of cell proliferation and differentiation must be tightly coordinated and balanced. Early on, proliferation must dominate, to allow the hindbrain to grow to the required size. Later on, as more cells differentiate and exit the cell cycle, the growth should cease. We explored the spatiotemporal features controlling this balance in the hindbrain boundary regions during this transition period, to gather information on population dynamics and cell lineage relationships. We made use of the Tg[BCP:H2AmCherry;CAAX:GFP] embryos, in which the cell plasma membranes are marked in green and the boundary progenitor cell nuclei and their derivatives, in red. We imaged embryos with light sheet fluorescence microscopy from 32 hpf to 45 hpf (Video 1), and we next studied the single cell behavior of the boundary progenitors by tracking their position over time. This allowed us to reconstruct the lineage of boundary cells concomitantly with the hindbrain morphogenetic changes (Figure 4A).

First, we assessed the impact of brain morphogenesis in the position, and therefore the fate, of boundary cells by tracking them and systematically assessing individual cell position and tissue movements over time. We observed that, as the hindbrain grew and underwent morphogenesis, boundary cells continuously proliferated (Video 1). Figure 4B shows transverse views of the hindbrain in an example of selected time frames; here, the cells in the boundary are depicted as dots and are plotted on top of a virtual hindbrain transverse section, with the shape of the ventricular surface color-coded. We observed an increase in the number of boundary cells over time (as an example, at t0 [33.4 hpf] = 103 cells vs. tf [44.7 hpf] = 155 cells), and changes in the shape of the ventricular surface. The dynamic analysis revealed the flattening of the ventricular surface as the neural tube grew (Figure 4C; note that the ventricular surface at the indicated time is depicted in color when overlaid on the ventricular surfaces corresponding to the different stages over the entire movie). We could better observe this change in shape by plotting the overlaid ventricular surfaces color-coded according to time (Figure S5A). This change resulted from the generation of the brain

ventricle (Lowery and Sive, 2009), which impacted as well the position of the progenitor cell population (Figure 2B; see scheme in Figure 4A). Moreover, this displacement of the boundary progenitors coincided with the increase in the neuronal differentiated population (Figure 1A-C; Voltes et al., 2019), such that progenitors were squeezed into the space between the ventricular surface and the neuronal differentiation domain. Measuring this displacement in the whole progenitor cell population, we could observe how progenitor cells shifted their position towards the dorsal domain (Figure S5B). As the displacement measurement of all tracked boundary cells along the medio-lateral (ML) axis did not result in significant changes of cell positions (Figure S5C), we conclude that not much cell intermingling occurred along this axis.

The analysis of the whole boundary proliferation dynamics at single-cell resolution revealed that boundary cells did not shut down their proliferative capacity (Figure 4D). For this, we analyzed the lineages of progenitor cells —those in the most ventricular domain— undergoing division or non-dividing. Cells were classified as non-proliferative if they did not divide after following them for more than 8 h, which is the estimated average time for a hindbrain cell to divide (Lyons et al., 2003). We observed that, during this period, approximately 60% of the boundary cells divided (Figure 4D; n = 73/120 cells). The cell lineage tree allowed us to reveal that boundary cell progenitors remaining in the ventricular domain did not stop their proliferative activity during this time interval (Figure 4D). Thus, although cells undergo differentiation, the boundary progenitor population is maintained.

Next, we wanted to analyze whether the different cell modalities (proliferative vs. non-proliferative) were located in specific domains in the boundaries. For this, we color-coded each cell according to its proliferative capacity, and plotted the cells' positions within the boundary over the entire time window. Mapping revealed that the cells did not display any specific distribution in the boundary; for instance, see proliferative blue vs. non-proliferative grey cells plotted at t0 and tf, in dorsal and transverse views, and that cells with different proliferative activities intermingled within the boundary (Figure 4E-E'). Moreover, this cell lineage analysis allowed division time and position within the boundary to be ascribed. When proliferative boundary cells that were color-

coded according to the time they divided (early vs. late) were mapped within the boundary, we observed that progenitors were not distributed in specific domains with respect to their time of division, and that they were intermingled (Figure 4F). This strongly suggests that boundary cells constitute a pool of actively proliferating progenitors at the same time they produce neurons. Moreover, it indicates that spatial and temporal features do not play a relevant role in conferring different cell behaviors in terms of proliferative capacity during this time interval.

Boundary cells display different division modes

Constant cell proliferation and active neurogenesis are intertwined during tissue growth. To understand the lineage relationship between them, we explored whether the neurogenic committed cells that reside in the boundaries could emerge from the multipotent neural stem cells after division, considering the possible division modalities: symmetric, asymmetric, or a mixture of the two. For this, we followed *in vivo* the derivatives of each single proliferative boundary cell after division and classified them according to i) the relative position of the two derivatives (besides or underneath), and ii) their location at tf, such that cells located in the ventricular zone were considered as progenitors, and cells in the mantle zone, as differentiated neurons. For instance, the behavior of two adjacent proliferative progenitors over time can display different division modes, as depicted in Figure 5A: one gave rise to two progenitor cells (PP) by symmetric division, while the neighboring one gave rise to a progenitor and a neuron (PN) by asymmetric division. When this analysis was performed in the whole boundary cell population, we observed that proliferative progenitors displayed both modes of division during this entire time interval, with no obvious preference for symmetric or asymmetric divisions (Figure 5B; SyD, n = 24/73 cells; AsyD, n = 30/73 cells; or unclassified n = 19/73 cells, when the derivatives were not able to be tracked for a long enough time to determine their fate). Next, we investigated whether different division modes were allocated specifically to distinct boundary domains. Strikingly, cells displaying both division modalities intermingled within the boundary (Figure 5C-C'; see maps at t0 and tf as examples). Thus, the cell position within the boundary was not relevant for these cell division behaviors. Almost

all symmetric divisions were self-renewable, giving rise to two progenitors (PP), since both daughter cells remained very dorsally located (Figure 5A, C-C', orange cells). We found only two symmetric divisions that generated two neuronal derivatives (NN) (Figure 5C'; see grey cells in the differentiated domain at tf); in both cases, the division occurred later than 40 hpf. Progenitors and derivatives after division were color-coded according to the conferred cell fate (Figure 5D-D'). When Tg[BCP:H2AmCherry] embryos were stained for Sox2 and HuC, we observed coherent proportions and position of progenitors and neurons within the whole population with the cell lineage analysis (compare Figure 5E-E' with D'). Furthermore, cell-renewal divisions during this period maintained the pool of progenitor cells within the boundaries despite the exiting of differentiated neurons. For instance, at t0, there were 97 progenitors (43 non-dividing cells, 24 symmetrically dividing progenitors, 30 asymmetrically dividing progenitors), and at tf, there were 117 progenitors (43 non-dividing cells, 44 progenitors arisen by symmetric division, 30 progenitors arisen by asymmetric division) plus 34 differentiated neurons. To understand how these cell fate decisions impacted the overall tissue, we mapped the trajectories of the whole cell population over time by calculating the average distance of all cells to the ventricular surface at each time point and plotting them over time, color-coding them according to their cell fate (Figure 5F). We observed a collective shift of the progenitor cell population towards the ventricular surface (Figure 5F, blue line), compatible with the displacement of the progenitor domain previously observed (Figure S5B) and its compaction between the ventricular surface and the neuronal differentiation domain. In contrast, neurons were clearly far from the ventricular zone as they moved towards the basal domain (Figure 5F, green line). Notably, this migration occurred from 40 hpf onwards, suggesting that most of the neuronal differentiation events in the boundaries occurred after 40 hpf, coinciding with the time period in which we observed the gross growth of neuronal differentiated domain. This analysis provided us with an informational system along temporal and spatial axes at the cell population level and indicated that boundary cells behaved in a non-synchronized manner: whereas some continue to divide symmetrically, others are already dividing asymmetrically and supplying neurons to the differentiated domain.

Boundary cells are fated to become neurons

Boundary cells continuously proliferate combining different division modes. To determine whether this proliferative capacity is maintained over longer periods of time, we quantified the differentiated neurons derived from boundary neural progenitors and the remaining progenitors at two different stages of embryonic development, namely, at 48 hpf and 72 hpf. Analyzing Tg[BCP:H2AmCherry] embryos stained with Sox2 and HuC, we observed that an average of 33% of the boundary mCherry-cells were in the neuronal differentiation domain and expressed HuC (Table 3; [51/156 cells] as an example of r5/r6); whereas at 72 hpf, 84% of the boundary derivatives were HuC positive (Table 3, [159/189 cells] as an example of r5/r6). This percentage reflected a dramatic increase in differentiated neurons originating from the boundary progenitors at 72 hpf (Figure 6A, Table 3). This resulted in an almost depletion of progenitor cells in the boundary, as observed by the Sox2-staining (Figure 6A, see blue staining at 48 hpf but no blue staining at 72 hpf; Figure 6B), indicating that the fate of the boundary cells is to become neurons.

The overall number of mCherry-positive cells (boundary progenitor cells and their derivatives) did not significantly change during this time, although at 72 hpf most cells were in the neuronal differentiation domain (Table 3). This suggests that boundary cells may undergo a massive neuronal differentiation with no need of cell division during this last time interval (48–72 hpf). The analysis of Sox2 progenitors along the hindbrain showed an enrichment in the most lateral domains with no apparent differences between rhombomeres and boundaries (Figure 6B), suggesting that a pool of long-lasting progenitors might reside in these lateral regions, but which do not exclusively rise from boundary cells.

To decipher whether boundary cells were fated to a particular neuronal identity, we analyzed the expression of specific neuronal differentiation markers, such as *lhx1a* and *evx1* (Belzunce et al., 2020). We did not observe differences in the expression of these genes between boundaries and rhombomeres; indeed, boundary derivatives expressed the differentiation marker corresponding to their specific mediolateral position (Figure 6C-D). These results indicated that boundary cells are unlikely to be fated to a particular neuronal identity distinct than those of the neighboring territories

and suggested that boundary cells eventually undergo differentiation to contribute to the refinement of the number, identity, and proportion of neurons in the hindbrain.

DISCUSSION

By reconstructing the lineage of hindbrain boundary cells, we determined i) the functional transition that this cell population undergoes; ii) the impact of morphogenesis in the spatial distribution of boundary cell progenitors, and iii) the general cellular/population dynamics. These results now provide the cellular data to complement the well-described gene regulatory networks involved in neuronal specification and differentiation in other biological contexts. Notably, we can use our CRISPR-based knock-in transgenic lines to specifically label the hindbrain boundary cell population, which provides for the first time the tools to reconstruct its lineage and explore its fate and behavior.

To ensure the robust outcome of a functional hindbrain with the precise number of neurons arranged in a precise topology, the neurogenic capacity is differentially allocated according to the position of the progenitor populations along the anteroposterior (AP) axis. Rhombomeric cells seem to engage very early in neurogenesis, such that the first neurogenic phase in the hindbrain is contributed by rhombomeric progenitors (Nikolaou et al., 2009; Gonzalez-Quevedo et al., 2010), whereas boundary cells are delayed in their neurogenic commitment. Indeed, boundary cells display crucial functions during early steps of hindbrain development (see review, Pujades, 2020). Thus, boundary cells are kept as neuroepithelial progenitor cells for a longer period than rhombomeric regions, and can actively proliferate by undergoing symmetric divisions to expand the stem cell pool in a Yap/Taz-TEAD-dependent manner (Voltes et al., 2019). There is no Notch activity in these cells when they act as mechanosensors, whereas Notch is highly active in the adjacent regions. During this period, they display specific molecular markers; however, these particular markers disappear at the time that the early-functions of the hindbrain boundaries are no longer required, coinciding with the onset of Notch activity around 32 hpf. Hereafter boundary cells switch their behavior acquiring radial glia properties and asymmetrically divide to become neurogenic (see model in Figures 6E and 6F). At this time, the Notch-pathway components *notch3-deltaD* are expressed in a pattern compatible with a canonical lateral inhibition mechanism operating at the

dorsoventral level. The most dorsal cells facing the ventricle were Notch-active, expressed Sox2, displayed zrf1, and proliferated asymmetrically, whereas the cells underneath expressed *delta* and proneural genes and eventually differentiated into neurons. Thus, the most plausible explanation is that this functional switch in Notch-activity results in the transition of boundary cells from a restricted symmetric division mode to an acquired asymmetric division capacity, which is crucial to maintain the balance between proliferation and differentiation. However, what triggers Notch-activity in the boundaries at that given moment is still an unanswered question.

Using high-resolution *in vivo* imaging, we could track the boundary cells while keeping morphology and spatial information. Our cell lineage analyses revealed that boundary cells supply differentiated neurons to the hindbrain through the transition to the asymmetric division mode, thereby maintaining the pool of boundary progenitors. Previous studies using single-cell clonal analyses in the whole hindbrain suggested that the majority of hindbrain neurons are born from symmetric neurogenic divisions — independently of the cell position along the AP axis— and that only a small percentage of asymmetric divisions occur (Lyons et al., 2003). The strength of our strategy is that we can live-monitor the behavior of the entire boundary cell population, which allowed us to go beyond lineage data and determine cellular trajectories (for instance); in other words, we were able to elucidate the emergent properties of entire cell populations. As boundary cells constitute a small proportion of hindbrain progenitors, it is possible that the clonal analyses of Lyons et al. (2003) contained a small number of boundary cells, and that the observed asymmetric divisions corresponded to boundary cells. This would suggest that whereas the main part of the hindbrain favors mainly symmetric neurogenic divisions, boundaries would behave different and be able to contribute to the growth by asymmetrically dividing. However, we suggest instead that progenitor cell capacities are distributed in the hindbrain all along the AP axis, which can be unfolded over time, in such a manner that boundary cells can behave as rhombomeric cells but in a delayed manner: rhombomeric progenitor cells would be the main contributers to neurons in the first phase of neurogenesis, and boundary cells would participate later. Thus, although the different progenitor pools along the AP axis are not synchronized, they might share a similar program, as is observed in other contexts for regulating the growth of the tissue: expanding the stem cell niche

(symmetric self-renewing divisions), maintaining the progenitor pool (asymmetric divisions), and finally differentiating neurons (either by symmetric neurogenic divisions or terminal differentiation) (see reviews, Shimojo et al., 2008; Sueda and Kageyama, 2019). To address this, similar *in vivo* analyses should be performed at earlier stages in the rhombomeric territories, to see whether indeed all progenitor cells in the hindbrain behave similarly and can display all proliferation modalities. Notably, we observed that boundary cells are unlikely to provide specific neuronal identities, but that boundary derivatives acquired their neuronal identity according to the Cartesian grid they interpreted —in other words, according to their positional information. This observation, together with the fact that boundary progenitors are mostly exhausted by 72 hpf, suggests that boundary cells after asymmetric division may end up differentiating and are required for supplying neurons to adjust the final number and proportions, more than for defining new neuronal subtypes. Interestingly, it indicates that overall neurogenesis would require a less tight regulation because the system could be finally adjusted by cells deriving from adjacent regions. Therefore, boundary cells would work fine-tuning the neuronal population. Whether this proliferative capacity remains beyond 72hpf by a remaining small fraction of putative progenitors is definitively a possibility (we did not address this here due to technical constraints). However, we cannot rule out an alternative scenario in which this later phase of neurogenesis would provide different neuronal subtypes contributing to the lineage diversity, such as it happens in the cortex (for review see Beattie and Hippenmeyer, 2017). As we do not know yet how and when different neural types are produced in the hindbrain, this is still a plausible consideration.

A question that now remains to be addressed is how this diversity arises from groups of “equivalent” boundary progenitor cells. While a body of previous work had suggested an orderly deterministic program for progenitor cell fate decisions in the mammalian cortex (Gao et al., 2014), a more stochastic model is currently favored (Llorca et al., 2019). The stochastic model has also been shown in the adult zebrafish telencephalon (Than-Trong et al., 2020), and the retina (He et al., 2012; Zechner et al., 2020). Our data showed that neither space nor time foretell the further behavior of boundary cells, suggesting that cell states and cell fates may be evenly distributed in the boundaries and thereby favoring a stochastic model.

Overall, by studying how the spatiotemporally coordinated cell progenitor specification and differentiation occurs alongside morphogenesis in the boundary cells, we revealed that time is a remarkable factor to organize stereotyped hindbrain growth, despite variability in proliferation modes. Functional analyses combining gene activity and cell lineage will be essential to understand molecular mechanisms involved in this neurogenic transition process. Resolving the lineage origin of cell types and combining it with the ascription of mutant phenotypes to specific lineages will be crucial to create these cell types on-demand.

MATERIALS AND METHODS

Zebrafish strains

Zebrafish (*Dario rerio*) were treated according to the Spanish/European regulations for the handling of animals in research. All protocols were approved by the Institutional Animal Care and Use Ethic Committee (Comitè Etica en Experimentació Animal, PRBB) and the Generalitat of Catalonia (Departament de Territori i Sostenibilitat) and were implemented according to European regulations. Experiments were carried out in accordance with the principles of the 3Rs.

Embryos were obtained by mating of adult fish using standard methods. All zebrafish strains were maintained individually as inbred lines. The Tg[βactin:HRAS-EGFP] line (termed Tg[CAAX:GFP] herein) expresses GFP in the plasma membrane and was used to label the cell contours (Dale and Topczewski, 2011). The Tg[tp1:d2GFP] line is a readout of cells with Notch activity, which expresses destabilized GFP under the control of *tp1* promoter (Clark et al., 2012). The Tg[HuC:GFP] line labels differentiated neurons (Park et al., 2000). Tg[atoh1a:GFP] (Belzunce et al., 2020) labeling the rhombic lip was generated by crossing Tg[atoh1a:KalTA4] (Distel et al., 2009) and Tg[UAS:GFP].

Generation of CRISPR-Cas9 knock-in transgenic line

The Gal4FF gene was inserted in one of the cis-regulatory elements (CRE) driving gene expression to boundary cells (Letelier et al., 2018). First, three sgRNAs (#1, #2 and #3) were designed to target the cis-regulatory element (CRE) located upstream of the *sgca* transcription start site (Figure S1A and SB). For this, the best hits provided by crisprscan.org and chopchop.cbu.uib.no platforms were used. Three sgRNAs (#1, #2 and #3) were synthetized as described in Gagnon et al., 2014 and their efficiency was confirmed by detecting indels in the genome target site. To do so, one-cell stage embryos were injected with each sgRNA in combination with Cas9 protein, and gDNA was extracted and amplified by PCR using Fw1 (5'- GAG AGA CCA CAC AGG GAA GC -3') and Hex-labeled Rv1 (5'- AGA GCA TAT ACA GAT CTA GGA AGA ATC -3') primers. The PCR product was subsequently sequenced by Gene Scan (Figure S1C). The presence of a multi-peak pattern indicates indels in the genome target site. sgRNA #2 displayed the best efficiency for digesting genomic DNA (40%). Gbait-hsp70:Gal4FF described in

Kimura et al., 2014 was used as donor vector and contains the eGFPbait (Gbait) as sgRNA target site, hsp70 promoter and Gal4FF (Figures 1D, S1A, and S1B). For generating the Gal4FF knock-in transgenic line, Tg[UAS:KAEDE] embryos at the one-cell stage were injected with 2 nl of a mix containing 50 ng/µl of each sgRNA (sgRNA #2 for digesting genomic DNA, and Gbait sgRNA for digesting the donor plasmid), 300 ng/µl of Cas9 protein with NLS (CP01-50 PNAbio) and 12 ng/µl of phenol:chloroform purified donor vector, so that concurrent double-strand breaks in the genomic target locus and the donor DNA could result in its integration at the target locus (see Figure S1 for a more detailed description of the knock-in pipeline, screening and genotyping strategy). The Gal4FF primers used were the following: Fw 5'- GCA GGC TGA AGA AGC TGA AG -3' and Rv 5'- GGA AGA TCA GCA GGA ACA GC -3' resulting in 59% efficiency (n = 16/27). Knock-in founders were selected by KAEDE-expression in F1 offspring and displayed a germline transmission rate of 25% (n = 4/16). 75% of these founders specifically expressed KAEDE in the boundaries (n = 3/4). Finally, adults were genotyped by fin clip using a strategy that confirmed integration and the insert directionality (Figure S1C); this involved a PCR with the following primers: Fw1 5'- GAG AGA CCA CAC AGG GAA GC -3'; Rv1 5'- AGA GCA TAT ACA GAT CTA GGA AGA ATC -3'; Fw2 5'- ATC GCA GAC CGA TAC CAG GA -3'; and Rv2 5'- TCG GGG AAA AAG TCC TGT CA -3'. The selected Tg[BCP:Gal4] fish used in this work contained 2 copies of the donor vector inserted in tandem (forward and reverse respectively). The Tg[BCP:Gal4;UAS:KAEDE] line (called Tg[BCP:KAEDE] along the manuscript) was outcrossed to segregate the UAS:transgene and isolate the Tg[BCP:Gal4]. After this, several transgenic lines were generated by crossing Tg[BCP:Gal4] fish with different UAS:reporter (UAS:GFP, UAS:H2AmCherry; Figure S1C). Specific expression was efficiently driven to the hindbrain boundaries (Figure 1E-1F). Certain leaky activity was appreciated in some ventrolateral cells in both boundaries and rhombomeres when Tg[BCP:Gal4] line was combined with UAS:KAEDE and UAS:GFP reporters, but not with UAS:H2AmCherry.

Whole mount *in situ* hybridization

Embryo wholemount *in situ* hybridization was adapted from Thisse and Thisse (2008). The following riboprobes were generated by *in vitro* transcription from cloned cDNAs: *deltaD* (Haddon et al., 1998) and *neurod4* (Park et al., 2003). *KAEDE*, *mCherry,* and

notch3 probes were generated by PCR amplification adding the T7 promoter sequence to the Rv primer: *KAEDE* Fw 5'- GCT GCT TAT GGA AGG CAA TG -3' and Rv 5'- CAA TCC AGA ATG GGC AAC AG -3'; *mCherry* Fw 5'- CCA AGC TGA AGG TGA CCA AG -3' and Rv 5'- GCT CGT ACT GTT CCA CGA TG- 3'; *notch3* Fw 5'- ATG GGG AAT TAC AGC CTT TG -3' and Rv 5'- GGC AAA CAA GCA CAT TCG TA -3'. *sgca* and *rfng* probes were generated as described (Letelier et al., 2018), *ascl1, lhx1a* and *evx1* as described (Belzunce et al., 2020), and *notch1a* as described (Taberner et al., 2020). For fluorescent in situ hybridization, FLUO- and DIG-labeled probes were detected with TSA Fluorescein and Cy3, respectively.

In toto embryo immunostainings

For immunostaining, 4% PFA-fixed embryos were permeabilized with 10 mg/ml proteinase K for different times according to the developmental stage (24–28 hpf, 5 min; 30–36 hpf, 10 min; 48–56 hpf, 20 min; 72 hpf, 30 min), blocked in 2% BSA, 5% goat serum, 0.1% Tween20 in PBS for 3 h at room temperature, and then incubated overnight at 4°C with the primary antibody. The primary antibodies used were: rabbit anti-GFP (1:500; Origene TP401), mouse anti-GFP (1:500; ThermoFisher A-11120), rabbit anti-Sox2 (1:100; Abcam ab97959), mouse anti-HuC (1:400, ThermoFisher A-21271), rabbit anti-Taz (1:150; Cell Signaling, D24E4), mouse anti-ZO1 (1:500 ThermoFisher ZO1-1A12), and zrf1 (ZDB-ATB-081002-46, ZIRC). After extensive washing with PBST, embryos were incubated overnight at 4°C with secondary antibodies conjugated with Alexa Fluor 488, 594, or 633 (1:500; Invitrogen). DRAQ5 (1:2000; Biostatus, DR50200) was used to stain nuclei.

Confocal imaging of whole mount embryos

Anesthetized, live embryos expressing genetically encoded fluorescence or stained fixed samples were mounted in 1% low melting point (LMP) agarose with the hindbrain positioned towards the glass-bottom of Petri dishes (Mattek) to achieve dorsal views of the hindbrain. Imaging was performed on a Leica SP8 inverted confocal microscope using a 20× objective (NA 0.7).

Light sheet imaging for cell lineage analysis

Anesthetized, live double-transgenic Tg[BCP:H2AmCherry;CAAX:GFP] embryos were mounted individually in 1% LMP-agarose in glass capillaries. During imaging, the embedded embryo was extruded from the capillary into the chamber filled with fish water. Time-lapse imaging was performed at 23°C on a Luxendo (Bruker) MuVi SPIM microscope using 22.2× objective for 16–18 h. Afterwards, the embryonic developmental stage was corrected accordingly (at 23°C development is delayed about 0.7-fold). Cell nuclei and plasma membranes channels were simultaneously recorded for the entire system every 5 min (Figure 4A, Video 1; ID: 181219).

3D+time cell lineage analysis pipeline

Image pre-processing

Image pre-processing was done using Fiji software (NIH). h5 files were converted into 16-bit tiff files using Big Data Processor tool and then cropped to focus on a single hindbrain boundary region. To compensate for small drifts of the embryo during image acquisition, a semi-automated rigid registration was carried out using developed FIJI-scripts (Dyballa et al., 2017). To improve signal to noise ratio on the nuclei BCP:H2AmCherry channel, the signal of the plasma membranes (CAAX:GFP) was subtracted and the resulting images were used for cell tracking analysis.

Cell tracking analyses

For cell-tracking analyses, all boundary cells of the datasets were reconstructed at single-cell resolution using MaMuT software (Massive Multi-view Tracker software (Wolff et al., 2018). Note that deep- and detailed analyses were performed in one dataset (ID: 181219-r5r6A), and those observations and conclusions were supported with partial analyses of additional datasets. Annotated spots were linked and tracked over time from 33.4 hpf (t0) to 44.7 hpf (tf), every 3.5 min, giving a total of 194 timeframes (ID: 181219-r5r6A-1). A total of 120 tracks were followed and classified according to: i) cell proliferative capacity (proliferative when the cell undergoes division, or non-proliferative when the cell does not divide in a period longer than 8 h), and ii) cell fate (progenitor, if the cell localized in the ventricular domain in tf, or neuron, if the cell localized in the mantle zone in tf). The following cell categories were considered: i) non-proliferative progenitors (NP, n = 26), ii) progenitors dividing symmetrically (SyD, n = 24), generating either two progenitors (PP, n = 22/24) or two

neurons (NN, n = 2/24); iii) progenitors dividing asymmetrically (AsyD), generating one progenitor and one neuron (PN, n = 30); and iv) committed neurons (CN, n = 20) when a non-dividing cell migrated to the mantle zone during the tracking. Twenty tracks were excluded from the cell fate classification for not allowing a clearly defined localization at tf (ID: 181219-r5r6-2).

Spots within the tracks were then grouped into selections and displayed with different appearances using the 3D-viewer of MaMut software (ID: 181219-r5r6A-2 to 5). Cell lineages and division events were also displayed in a hierarchical way as lineage trees using the Tracking scheme or using the basic graphical functions of R. The numerical features of each single spot (cell), such as spot location, division time, and spot ID, were exported into csv files for further computational analyses.

Morphogenetic studies

The plasma membrane channel (CAAX:GFP) was used to model the neural tube volume in a representative fraction of time-frames (45 timepoints, from frame t0 to frame tf, every 17.5 minutes). The dorsal surface of the neural tube facing the ventricle (or ventricular surface) was plotted using Surface tool on Imaris 8.4.2, and the 3D-coordinates were exported in WRL file format to make computations. Data were converted to PLY file format using *meshlabserver 2020.07* (Cignoni et al., 2008). Once the triangular mesh read into `R` (R core team 2020) and using packages `rgl` (Adler and Murdoch, 2020) and `Rvcg` (Schlager, 2017), some parts were clipped to obtain the interesting component of the mesh that included the ventricular surface. From this, the vertical sections at coordinate Y=39 were obtained (Figures 4 and S5).

Cell trajectory analysis

Data on cell positions within the hindbrain were obtained from the csv files generated by MaMut as $X_t = (x_t, y_t, z_t) \in R^3$, ($x_t$: lateral/medial/lateral, y_t: anterior/posterior, and z_t: dorsal/ventral). Coordinates were measured in micrometers. To make it easier to interpret, the averages of each cell's positions were computed (Figure S4). To compute distances from a given cell at a given time (t) to the ventricular surface, the given ventricular surface was selected for the closest available time; from this, the vertex with minimum Euclidean distance to the cell position was calculated. That minimum distance was taken as the distance from the cell position to the ventricular surface.

Pharmacological treatments

Tg[BCP:H2AmCherry;HuC:GFP] sibling embryos were treated either with 10 μM of the gamma-secretase inhibitor LY411575 (Stemgent) or DMSO for control. The treatment was applied into the fish water at 28.5°C from either 20 hpf to 26 hpf, or 30 hpf to 36 hpf. After treatment, embryos were imaged *in vivo* under a Leica SP8 confocal microscope.

Quantifications and statistical analysis

For assessing the percentage of neurons derived from the boundary cell population (Figure 2C) and the percentage of boundary cells displaying Notch activity (Figure 2F), we quantified the number of cells expressing mCherry with or without GFP in a constant ROI. This ROI covered the whole BCP in every analyzed boundary using Tg[BCP:H2AmCherry;HuC:GFP] or Tg[BCP:H2AmCherry;tp1:d2GFP] embryos (Tables 1, 2). No significant changes were observed when comparing different boundaries from r2/r3 to r5/r6 (Table 2). Thus, for further quantifications we limited our analysis to r4/r5 and r5/r6 and represented r5/r6 in box-plots (Figure 2C, 2F). For quantifying the percentage of neurons derived from the BCP at 48 and 72 hpf (Figure 6A), we immunostained Tg[BCP:H2AmCherry] embryos with anti-Sox2 and anti-HuC and quantified the number of cells expressing mCherry with or without GFP in a constant ROI covering the whole BCP (Table 3). Mean, standard deviation, and standard error of mean are shown in each case using unpaired t-test with Welch's correction (*$p < 0.05$, ****$p < 0.0001$).

ACKNOWDELGEMENTS AND FUNDING SOURCES

The authors thank Gopi Shah at the Mesoscopic Imaging Facility at EMBL Barcelona for helping with SPIM imaging, Juan Manuel Fuentes at the Scientific-IT (DCEXS-UPF) for helping with computational analysis, and Sebastien Tosi (IRB, Barcelona) and members of the ALMU facility (CRG-UPF, Barcelona) for technical support during image processing. We also thank S Higashijima for kindly providing the Gal4 donor vector plasmid for generating the CRISPR/Cas9 knock-in. We like to thank Laia Subirana and Marta Linares for technical assistance, Gonzalo Ortiz-Alvarez and other current members of the lab for insight and critical discussions, and Isabel Espinosa-Medina and Esteban Hoijman for critical reading of the manuscript. This work was funded by the Agencia Española de Investigación AEI-PGC2018-095663-B-I00 and RED2018-102553-T grants (MICIU-FEDER) to CP. DCEXS-UPF is a Unidad de Excelencia María de Maeztu funded by the AEI (CEX2018-000792-M). CEP is a recipient of a predoctoral FPU fellowship from the Spanish Ministry of Universities. FU work was supported by PGC2018-101643-B-I00 (MICIU-FEDER). CP is a recipient of ICREA Academia award (Generalitat de Catalunya).

AUTHOR CONTRIBUTIONS

CFH and CP contributed to the concept and design of experiments, interpretation of the results and wrote the manuscript. CFH and CEP performed and analyzed the experiments and interpreted the results. FU collaborated with CFH in the mathematical analysis of data.

CONFLICT OF INTERESTS

The authors declare no competing interests.

FIGURE LEGENDS

Figure 1: Neurogenesis in boundary cells is delayed compared to neighboring rhombomere domains.

(A–C) Double immunostaining of wild-type embryos at different stages with the neural progenitor marker Sox2 (magenta), and the pan-neuronal differentiation marker HuC (green). Dorsal maximum intensity projections of the Z-stacks covering the boundary cell population are shown, with anterior to the top. Inserts, dorsal view magnifications of framed regions, with the overlay of both channels (top), only Sox2 (middle), or only HuC (bottom). Note that the boundaries display a higher accumulation of Sox2 as compared to the rhombomere-flanking regions at 32 and 48 hpf. a-c, a'-c') transverse single-stack views at the level of rhombomeres or boundaries, respectively. Note that the HuC domain increases over time. (D) CRISPR/Cas9 knock-in strategy to generate the zebrafish Tg[BCP:Gal4] line. (E) Tg[BCP:KAEDE] embryos at 36 hpf display specific expression in the MHB and in the hindbrain boundary cells. DNA is labeled by DRAQ5 in grey. (F) Tg[BCP:KAEDE;elA:GFP] embryo at 36 hpf expressing GFP in rhombomere (r) 3 and (r) 5, and KAEDE in the boundary cells. (G–I) Spatiotemporal characterization of the Tg[BCP:H2A-mCherry] line; dorsal views are shown, with anterior to the top. g-i) transverse views of (G–I) at the level of the indicated boundary (see dashed line). White arrows in (i) indicate neuronal derivatives of boundary cells. Note that the onset of H2A-mCherry in the boundaries is around 24 hpf, and that H2A-mCherry is maintained until much later stages specifically in the boundary cells and their derivatives, excluding the rhombic lip cells. (J) Tg[atoh1a:GFP] embryo with DRAQ5, which stains the cell nuclei; (j) the transverse view is shown at the level of the indicated boundary (see dashed line). Note that GFP is restricted to the rhombic lip (Kidwell et al., 2018). (K) Scheme depicting the expression of atoh1a (green), the Sox2-domain in blue, and the boundary cells labeled by the knock-in line (magenta); k), transverse view at the level of the indicated boundary (see dashed line) showing that the domains of atoh1a and the boundary cells not fated to the rhombic lip do not overlap. Unless stated, embryos are displayed as dorsal maximum intensity projections (MIP) with anterior to the top. Transverse views as MIP of a single boundary. White arrowheads indicate the position of the hindbrain boundaries. BCP, boundary cell

population; MHB, mid-hindbrain boundary; hpf, hours-post fertilization; ov, otic vesicle; rl, rhombic lip. Scale bar, 50 μm.

Figure 2: Boundary progenitor cells undergo neuronal differentiation in a Notch-dependent manner

(A, B) Tg[BCP:H2A-mCherry;HuC:GFP] embryos at different developmental stages; a-b) transverse views at the level of the indicated boundary (see dashed line). Inserts (both dorsal and transverse views) display magnifications of framed regions, with the overlay of both channels (top), only boundary cells (middle), or only HuC (bottom). Note that at 30 hpf, boundary cells are in the ventricular domain and do not display HuC, whereas at 48 hpf, several boundary cells are in the neuronal differentiated domain (see white arrow in transverse view inserts). (C) Boxplot showing the % of neuronal differentiated boundary cells at 30 or 48 hpf (Table 1); ****$p < 0.0001$. (D, E) Tg[BCP:H2A-mCherry;tp1:d2GFP] embryos at different developmental stages; d-e) transverse views at the level of the indicated boundary (see dashed line in D-E). Inserts (both dorsal and transverse views) display magnifications of framed regions, with the overlay of both channels (top), only boundary cells (middle) or only Notch-active cells (bottom). Note that boundary cells are devoid of Notch activity at 26 hpf but most have Notch activity at 48 hpf (see white arrow in transverse view inserts). (F) Boxplot showing the switch in Notch activity in the boundary cells (Table 2). ****$p < 0.0001$. (G) Experimental design for loss of Notch function experiments, depicting the shape of the hindbrain in transverse views at the distinct developmental stages. (H–K) Transverse views of Tg[BCP:H2A-mCherry;HuC:GFP] embryos treated from either 20–26 hpf (H-I; DMSO n = 3/3 embryos; LY411575 n = 4/4 embryos) or 30–36 hpf (J-K; DMSO n = 5/5 embryos; LY411575 n = 4/4 embryos), with DMSO (H, J) or the gamma-secretase inhibitor LY411575 (I, K). For (I, K), note that boundary cells do not express HuC if treated before the onset of Notch-activity (I) but do express HuC if treated after the onset of Notch-activity (K). Unless stated, embryos are displayed as maximum intensity projections (MIP). Transverse views as MIP of a single boundary. In (A, B, D, E), dorsal views are shown, with anterior at the top. White arrowheads indicate the position of the hindbrain boundaries. BCP, boundary cell population; hpf, hours-post-fertilization. Scale bar, 50 μm.

Figure 3: Notch players are expressed in the boundary cells from 36 hpf onwards.

(A–D) Tg[BCP:GFP] embryos, before and after the onset of Notch activity in the boundary cells, were used for double *in situ* hybridization with: (A, B) *notch3* and *deltaD* followed by an anti-GFP staining to detect the boundary cells. a-a'''', b-b''''), transverse views of the boundary indicated by the dashed line in (A, B), and display either single staining or several combinations according to the color-coded labeling. Inserts display magnifications of a single-stack view of the framed region. Note that *notch3*-positive cells are more dorsally located than *deltaD*-positive cells, and the stained cells never overlap; and (C-D) double *in situ* hybridization with *ascl1a* and *neuroD4*, followed by an anti-GFP staining to detect the boundary cells. c-c'''', d-d''''), transverse views through the indicated boundary, displaying either single staining or several combinations according to the color-coded labelling. Inserts display magnifications of a single-stack view within the framed region. Note that at 26 hpf, none of the boundary cells displayed any of the proneural genes, whereas at 36 hpf, some boundary cell–derivatives express *ascl1a* and *neuroD4*. Unless indicated, embryos are displayed as maximum intensity projections (MIP) with anterior to the top. White arrowheads indicate the position of the hindbrain boundaries. BCP, boundary cell population; hpf, hours-post-fertilization. Scale bar, 50 μm.

Figure 4: Boundary cells display proliferative capacity.

(A) Scheme depicting the outline of the experiment: Tg[BCP:H2AmCherry; CAAX:GFP] embryos were imaged in a light sheet fluorescence microscope over a period encompassing progenitor cell proliferation, neuronal differentiation, and tissue morphogenesis (32–45 hpf). (B) Spatial map of a single boundary (in transverse view) with annotated nuclei from boundary cells (grey dots) displayed on the top of neural tube masks (represented as grey surfaces), showing the position of all cells at the given time. The corresponding segmented ventricular surface was color-coded according to embryonic time (33.4 hpf, purple; 36.6 hpf, blue; 40.8 hpf, turquoise; 44.7 hpf, light green). (C) Dynamic comparison of the segmented ventricular surface of rhombomere 5 over time from framed regions in (B), displaying in the same color-coded manner than in (B) the shape of the surface at the given embryonic stage on the top of the 45 different analyzed time frames (in grey hues). (D) Flat representation of boundary cell

lineage tree in which each line corresponds to a single cell from the moment of tracking onwards that bifurcate upon cell division. An interrupted line indicates either that the movie ended or that the cell was lost from the field. The X-axis displays the time of embryonic development (hpf). Boundary cell lineages are color-coded according to proliferative behavior (blue, dividing; grey, non-dividing). (E, F) Spatial map of a single boundary (in dorsal or transverse view) displaying the regions framed in (B), with annotated nuclei from all boundary progenitors shown in (D) and displayed at t0 (33.4 hpf; E) and/or tf (44.7 hpf; E' and F). The maps were built after following the lineages of all boundary cells during this time interval. In (E-E'), cells were color-coded according to the same criteria than in (D). and displayed at t0 (33.4 hpf) and tf (44.7 hpf). Note that different cell proliferative capacities are not specifically allocated within the boundary. (F) Spatial map of a single boundary (in dorsal or transverse view displaying the regions framed in (B) with annotated nuclei from dividing progenitor cells color-coded according to time of division (33.4–36.6 hpf, purple; 36.6–40.8 hpf, turquoise; 40.8–44.7 hpf, yellow). Note that time of division does not correlate with specific spatial domains within the boundary. BCP, boundary cell population; hpf, hours-post-fertilization.

Figure 5: Proliferative boundary progenitor cells undergo both symmetric and asymmetric division.

(A) Example of two neighboring progenitor cells (dorsal and transverse views) undergoing distinct division modes. Orange arrowheads indicate the progenitor cells that will divide symmetrically giving rise to two daughter cells remaining in the progenitor domain (P); blue arrowheads indicate the progenitor cell that will asymmetrically divide giving rise to two daughters, one progenitor (P, blue) and one neuron (N, green arrowhead); white asterisk, the time frame in which the cell divides. (B) Flat representation of proliferative boundary cell lineage tree. Each line corresponds to a single cell from the moment of tracking onwards that bifurcate upon cell division. The X-axis displays the time of embryonic development in hours-post-fertilization (hpf). Boundary cell lineages are color-coded according to mode of division (orange, symmetric; blue, asymmetric). An interrupted line means that the cell was lost from the field. Note that approximately half of the proliferative boundary cells

divide symmetrically and the other half, asymmetrically. (C, D) Spatial map of a single boundary (in dorsal or transverse view displaying the regions framed in Figure 4B) with annotated nuclei from all boundary progenitors shown in (B) and color-coded according to mode of division (C) and cell fate (D). In C), orange, symmetric progenitor division; grey, symmetric neurogenic division; green: asymmetric division). In D), blue, progenitors; green, neurons. Images were taken at t0 (33.4 hpf; C-D) and tf (44.7 hpf; C'-D'). Maps were built after following the lineages of all boundary cells during this time interval. Note that different cell division modes as displayed in (C) are not specifically allocated within the boundary. (E-E') Tg[BCP:H2AmCherry;HuC:GFP] embryos at 48 hpf and immunostained with anti-Sox2 and anti-HuC. Note that boundary progenitor cells display Sox2 and some of their derivatives express HuC. (F) Graph displaying the average distance of the two cell populations deriving from boundary cells (progenitor vs. neuron) to the ventricular surface in micrometers (0, close to the ventricular surface; 30, far from the ventricular surface) at different embryonic stages (hpf). Note how progenitor cells (blue line) become closer to the surface, and how neuronal derivatives (green line) move away from the ventricular surface. BCP, boundary cell population; hpf, hours-post-fertilization.

Figure 6: The pool of boundary progenitors extinguishes over time.

(A) Boxplot displaying the % of neuronal differentiated boundary cells at 48 hpf or 72 hpf (Table 3). Note that at 48 hpf, magenta cells located in the ventricular zone displayed Sox2 (white arrows), and those below expressed HuC (green arrows); however, at 72 hpf, very few Sox2-positive cells were observed in the ventricular zone, and most boundary cells expressed HuC (Table 3). (B) Tg[BCP:H2AmCherry] embryos at 72 hpf were immunostained with Sox to assess the percentage of boundary cells that remained as neural progenitors. Note that very few boundary cells (blue) displayed Sox2 (grey). (C) Tg[BCP:GFP] embryos at 48 hpf were *in situ* hybridized either with *lhx1a* (B) or *evx1* (C). In all cases, dorsal views are displayed with anterior to the top; b-d) transverse views. (E) Illustration depicting the functional transition of the boundary cell population. At the beginning of neuronal differentiation (26 hpf), the cells within the boundary are neuroepithelial progenitors that divide symmetrically (purple cells). Notch-signaling is then activated after a short time (here, at 36 hpf) in the boundary

progenitor cells, singling them out (grey cell); these cells then undergo asymmetric cell division (similar to radial glia cells) and give rise to one progenitor (grey cell) and one committed neuroblast (blue cell), such that the pool of boundary cells is maintained while still contributing differentiated neurons to the tissue. By 48 hpf, the progenitor domain is reduced and squeezed between the ventricular surface and the neuronal differentiation domain; the most dorsally-located boundary cells still display Notch activity, whereas the previous committed neuroblasts are already differentiated into the neurons (green cells) of the boundary differentiation domain. Finally, at 72 hpf, the boundary progenitor cells are mainly exhausted. (F) Model explaining the boundary cell behavior during this time interval, and the corresponding associated molecular features. Boundary cells are specified at the interfaces between rhombomeres at early embryonic stages (18–20 hpf) and express different boundary markers (Amoyel et al., 2005; Letelier et al., 2018). They activate Yap/Taz-TEAD in response to mechanical stimuli to be maintained as proliferating progenitors (Voltes et al., 2019). By 32 hpf, boundary cells become Notch-active, and they can engage in neurogenesis. This Notch switch coincides with the acquisition of a new mode of cell division —asymmetric division, which allows boundary cells to provide differentiated neurons to the hindbrain. Accordingly, boundary derivatives display proneural genes and neuronal differentiation markers such as HuC. Finally, boundary cells most probably undergo direct differentiation, as the differentiation domain dramatically increases at the expense of the progenitor domain. White arrowheads indicate the position of the hindbrain boundaries. BCP, boundary cell population; hpf, hours-post-fertilization. Scale bar corresponds to 50 μm.

Video 1: Time-lapse of the boundary cell population.

Tg[BCP:H2AmCherry] embryo displaying mCherry in the boundary cell nuclei was imaged from 32 to 44.7 hpf. The movie shows the dynamics and behavior of a single embryo with all boundaries, and the insert focusses on a single boundary. Dorsal view with anterior to the top, with inserts of r5/r6 as indicated by the green box. Transverse view of r5/r6 boundary. BCP, boundary cell population; hpf, hours-post-fertilization. Embryo dataset ID: 181219.

Table 1: Percentage of boundary progenitor cells that underwent neuronal differentiation at different embryonic stages (**p < 0.0001).**

	% differentiated mCherry cells in Tg[BCP:H2AmCherry;HuC:d2GFP] embryos			
	r4/r5 (n = 5 embryos)		r5/r6 (n = 5 embryos)	
	30 hpf	48 hpf	30 hpf	48 hpf
Mean	1.9 [1.4/74 cells]	44.2 [77/174 cells]	1.6 [1.6/99 cells]	40.1 [79/197cells]
SD	2.6	4.2	1.5	5.2
SEM	1.2	2.1	0.7	2.3
p value	< 0.0001		< 0.0001	

Table 2: Percentage of Notch-active cells in Tg[BCP:H2AmCherry;tp1:d2GFP] embryos along the different boundaries at 26 hpf or 36 hpf (**p < 0.0001).**

A	% Notch-active mCherry cells in Tg[BCP:H2AmCherry;tp1:d2GFP] embryos			
	r4/r5		r5/r6	
	26 hpf (n=6 embryos)	36 hpf (n=4 embryos)	26 hpf (n=6 embryos)	36 hpf (n=4 embryos)
Mean	5.6 [2.2/39.8 cells]	54.7 [58/106 cells]	6.4 [2.6/40 cells]	63.8 [73/114 cells]
SD	5.2	5.1	6.3	8.7
SEM	2.2	2.5	2.6	4.4
p value	<0.0001		<0.0001	

B	% Notch-active mCherry cells in Tg[BCP:H2AmCherry;tp1:d2GFP] embryos							
	26 hpf (n = 6 embryos)				36 hpf (n = 4 embryos)			
	r2/r3	r3/r4	r4/r5	r5/r6	r2/r3	r3/r4	r4/r5	r5/r6
Mean	9.2	10.5	5.6	6.4	66.2	57.7	54.7	63.8
SD	5.9	6.2	5.4	6.3	7.6	10.3	5.1	8.8
SEM	2.6	2.5	2.2	2.6	3.8	5.2	2.5	4.4
p value	0.20 (ns)				0.24 (ns)			

Table 3: Percentage of boundary cells in Tg[BCP:H2AmCherry;HuC:GFP] embryos that underwent neuronal differentiation and the total number of boundary cells at different embryonic stages (*p < 0.001, ****p < 0.0001).**

A	% differentiated mCherry cells in Tg[BCP:H2AmCherry] αSox2 αHuC embryos			
	r4/r5 (n= 10 embryos)		r5/r6 (n=10 embryos)	
	48 hpf	72 hpf	48 hpf	72 hpf
Mean	37 [54/146 cells]	81 [136/168 cells]	32.8 [51/156 cells]	84.2 [159/189 cells]
SD	7.8	6.2	11.1	3.0
SEM	3.5	2.8	4.9	1.3
p value	<0.0001		0.0003	

B	Total number of mCherry cells in Tg[BCP:H2AmCherry] αSox2 αHuC embryos			
	r4/r5 (n= 10 embryos)		r5/r6 (n= 10 embryos)	
	48 hpf	72 hpf	48 hpf	72 hpf
Mean	145.6	168.2	156	188.8
SD	19.7	28.8	32.9	54.9
SEM	8.8	12.9	14.7	24.6
p value	0.19 (ns)		0.29 (ns)	

SUPPLEMENTARY MATERIAL

Supplementary Figure S1: Generating CRISPR/Cas9 knock-in transgenic lines to trace the boundary cell population

(A) Scheme depicting the CRISPR/Cas9 knock-in strategy. The boundary cell population cis-regulatory element (BCP-CRE) located upstream *sgca* transcription start site was targeted by CRISPR/Cas9; after inducing double-strand breaks, the donor vector carrying Gal4FF was integrated. Using the hsp70 promoter in the construct allowed both forward and reverse integrations to be functional. (B) Genomic description of the knock-in target site, before and after integration and repair, in one of the Tg[BCP:Gal4] founders (the one selected for this work). The sgRNA target site is indicated in blue; intergenic sequence, grey; and *sgca*, black (the coding region of the first exon is underlined). After efficiently knocking-in the target locus, two copies of the insert were integrated in tandem (orientation indicated with purple boxes; green sequence indicates a fraction of Gbait, and purple sequence the beginning of hsp70 promoter). Note the presence of small indels (grey sequence between the blue sequence of the endogenous locus and the integrated construct) indicating that homology-independent DNA repair occurred in the targeted locus. (C) CRISPR/Cas9 knock-in pipeline. Three sgRNA target sites (#1, #2, #3) were designed according to the best hits provided by the crisprscan.org and chopchop.cbu.uib.no platforms; these were synthetized, and their efficiency was confirmed by detecting indels in the genome target site. Tg[UAS:KAEDE] embryos at the one-cell stage were injected with a mix containing the two sgRNAs (sgRNA #2 for digesting genomic DNA, and Gbait sgRNA for digesting the donor plasmid), Cas9 protein and the donor DNA vector. Embryos were selected by mosaic KAEDE-expression (53% efficiency, n = 40/76). Successful Gal4 genome integration was confirmed in adult fish by PCR with Gal4FF primers and resulted in 59% efficiency (n = 16/27). Knock-in founders were selected by KAEDE-expression in F1 offspring and displayed a germline transmission rate of 25% (n = 4/16). 75% of these founders specifically expressed KAEDE in the boundaries (n = 3/4). Finally, adults were genotyped by fin clip using a strategy that confirmed integration and the insert directionality; this involved a combination of PCRs using Fw1, Rv1, Fw2 and Rv2 primers, so that the products A, B, C or D were amplified depending on the construct

orientation. The selected Tg[BCP:Gal4] fish used in this work showed a A+D+ genotype, indicating that it contained at least two copies of the donor vector inserted in tandem (forward and reverse). Subsequent sequencing of genomic DNA (gDNA) target site confirmed the tandem knock-in (see the sequence description in (B)). The Tg[BCP:Gal4;UAS:KAEDE] line (called Tg[BCP:KAEDE] in the manuscript) was outcrossed to segregate the UAS:transgene and to isolate Tg[BCP:Gal4]. After this, several transgenic lines were generated by crossing Tg[BCP:Gal4] fish with different UAS:reporter (UAS:GFP, UAS:H2AmCherry).

Supplementary Figure S2: Comparative analyses of the spatiotemporal profile of the boundary cell population markers and the Tg[BCP:H2AmCherry] transgene

(A–F) Double *in situ* hybridization of Tg[BCP:H2AmCherry] embryos at different stages with *sgca* and *mCherry.* Dorsal, transverse, or sagittal views are indicated for each case. Expression of *mCherry* was delayed with respect to *sgca* expression. (G–N) *In situ* hybridization with the boundary marker *rfng* in Tg[elA:GFP] embryos (a landmark of r3 and r5) at different stages, combined with the immunostaining of ZO-1, to label apical tight junctions. Note the offset of *rfng* between 31 and 33 hpf (M, N). (O, P) Double immunostaining of wild-type embryos at 30 hpf with Taz and ZO-1. Taz is expressed in the ventricular domain of the boundaries (Voltes et al., 2019); ZO-1 labelling allows the larger apical feet of boundary cells to be visualized (Symonds et al., 2020). Q-R) Transverse views of the Tg[BCP:H2AmCherry;4xGTIIC:d2GFP] embryos showing that mCherry-boundary cells display Yap/Taz-TEAD-activity at 33 hpf (Q-Q') and 48 hpf (R-R'). Inserts show Yap/Taz-TEAD active boundary cells (black asterisks) in the progenitor domain at 33 hpf and a fraction of their derivatives in the neuronal differentiated domain at 48 hpf (white asterisks). White arrowheads indicate the position of the hindbrain boundaries. BCP, boundary cell population; hpf, hours-post-fertilization; MHB, mid-hindbrain boundary. Scale bar, 50 μm.

Supplementary Figure S3: Rhombomeric expression of Notch-players

(A–I) Embryos displaying Notch-activity and Notch players in the rhombomeres at 26 and 36 hpf. (A, D) Tg[tp1:d2GFP] as a read-out of Notch activity. (B, E, G) Embryos hybridized with *notch3*. (C, F-H) Embryos hybridized with *deltaD*. (I) Embryos

hybridized with *notch1.* Transverse views are shown at the level of rhombomere 5. BCP, boundary cell population; hpf, hours-post-fertilization; rl, rhombic lip. Scale bar, 50 μm.

Supplementary Figure S4: Notch-active boundary cells display radial glia morphology

(A, B) Tg[BCP:H2AmCherry;tp1:d2GFP] embryos *in vivo* imaged (A) or immunostained with the radial glia marker zrf1 (B) at 48 hpf. Transverse view with inserts show the cell processes of Notch-active boundary cells towards the basal domain of the hindbrain (A), and equivalent Notch-active cells stained with anti-zrf1 (B, blue). Scale bar, 50 μm.

Supplementary Figure S5: Temporal representation of morphogenetic and cellular movements in the boundaries

(A) Dynamic representation of the changes in shape of the ventricular surface during morphogenesis. Overlay of segmented ventricular surfaces of the same embryo over time, color-coded according to time of development. Note the flattening that it undergoes as the neural tube grows, and the shift towards dorsal. Dorsal indicates the most dorsal part of the lumen closed by the epidermis, and ventral, the ventricular surface of the hindbrain. (B) Average movement of all boundary progenitor cells along the dorsoventral axis over time, measured by the μm of distance to the ventricular surface. Each frame corresponds to the average position of all individual progenitors. Note that the progenitors undergo a shift on their position towards dorsal (e.g., closer to the ventricular surface), coinciding in time with the increase in the neuronal differentiated population located in the ventral domain. (C) Cell movements along the lateromedial axis over time. The position of each single progenitor cells was tracked over time (black lines). Red lines represent the average position for the tracks grouped by hemisphere. Note that no relevant cellular movements were observed along this axis. D, dorsal; V, ventral; L, lateral; M, medial; hpf, hours-post-fertilization.

REFERENCES

Adler, D., Murdoch, D., 2020. Rgl: 3D Visualization Using OpenGL https://CRAN.R-project.org/package=rgl.

Amoyel, M., Cheng, Y.-C., Jiang, Y.-J., Wilkinson, D.G., 2005. Wnt1 regulates neurogenesis and mediates lateral inhibition of boundary cell specification in the zebrafish hindbrain. Development 132, 775–785. doi:10.1242/dev.01616

Beattie R, Hippenmeyer S. 2017. Mechanisms of radial glia progenitor cell lineage progression. FEBS Lett 591:3993–4008. doi:10.1002/1873-3468.12906

Belzunce, I., Belmonte-Mateos, C., Pujades, C., 2020. The interplay of atoh1 genes in the lower rhombic lip during hindbrain morphogenesis. PLoS ONE 15, e0228225. doi:10.1371/journal.pone.0228225

Calzolari, S., Terriente, J., Pujades, C., 2014. Cell segregation in the vertebrate hindbrain relies on actomyosin cables located at the interhombomeric boundaries. EMBO J. 33, 686–701. doi:10.1002/embj.201386003

Cheng, Y.-C., Amoyel, M., Qiu, X., Jiang, Y.-J., Xu, Q., Wilkinson, D.G., 2004. Notch activation regulates the segregation and differentiation of rhombomere boundary cells in the zebrafish hindbrain. Developmental Cell 6, 539–550.

Cignoni, P., Callieri, M., Italian, M.C.E., 2008, 2008. Meshlab: an open-source mesh processing tool. diglib.eg.org

Clark, B.S., Cui, S., Miesfeld, J.B., Klezovitch, O., Vasioukhin, V., Link, B.A., 2012. Loss of Llgl1 in retinal neuroepithelia reveals links between apical domain size, Notch activity and neurogenesis. Development 139, 1599–1610. doi:10.1242/dev.078097

Cooke, J.E., Kemp, H.A., Moens, C.B., 2005. EphA4 is required for cell adhesion and rhombomere-boundary formation in the zebrafish. Current Biology 15, 536–542. doi:10.1016/j.cub.2005.02.019

Dale, R.M., Topczewski, J., 2011. Identification of an evolutionarily conserved regulatory element of the zebrafish col2a1a gene. Developmental Biology 357, 518–531. doi:10.1016/j.ydbio.2011.06.020

Distel, M., Wullimann, M.F., Köster, R.W., 2009. Optimized Gal4 genetics for permanent gene expression mapping in zebrafish. Proc. Natl. Acad. Sci. U.S.A. 106, 13365–13370. doi:10.1073/pnas.0903060106

Dyballa, S., Savy, T., Germann, P., Mikula, K., Remesikova, M., Špir, R., Zecca, A., Peyriéras, N., Pujades, C., 2017. Distribution of neurosensory progenitor pools during inner ear morphogenesis unveiled by cell lineage reconstruction. Elife 6, 951. doi:10.7554/eLife.22268

Fraser, S., Keynes, R., Lumsden, A., 1990. Segmentation in the chick embryo hindbrain is defined by cell lineage restrictions. Nature 344, 431–435. doi:10.1038/344431a0

Gagnon, J.A., Valen, E., Thyme, S.B., Huang, P., Ahkmetova, L., Pauli, A., Montague, T.G., Zimmerman, S., Richter, C., Schier, A.F., 2014. Efficient Mutagenesis by Cas9 Protein-Mediated Oligonucleotide Insertion and Large-Scale Assessment of Single-Guide RNAs. PLoS ONE 9, e98186–8. doi:10.1371/journal.pone.0098186

Gao, P., Postiglione, M.P., Krieger, T.G., Hernandez, L., Wang, C., Han, Z., Streicher, C., Papusheva, E., Insolera, R., Chugh, K., Kodish, O., Huang, K., Simons, B.D., Luo, L., Hippenmeyer, S., Shi, S.-H., 2014. Deterministic progenitor behavior and unitary production of neurons in the neocortex. Cell 159, 775–788. doi:10.1016/j.cell.2014.10.027

Gonzalez-Quevedo, R., Lee, Y., Poss, K.D., Wilkinson, D.G., 2010. Neuronal regulation of the spatial patterning of neurogenesis. Developmental Cell 18, 136–147. doi:10.1016/j.devcel.2009.11.010

Guthrie, S., Lumsden, A., 1991. Formation and regeneration of rhombomere boundaries in the developing chick hindbrain. Development 112, 221–229.

Haddon, C., Jiang, Y.J., Smithers, L., Lewis, J., 1998. Delta-Notch signalling and the patterning of sensory cell differentiation in the zebrafish ear: evidence from the mind bomb mutant. Development 125, 4637–4644.

He, J., Zhang, G., Almeida, A.D., Cayouette, M., Simons, B.D., Harris, W.A., 2012. How variable clones build an invariant retina. Neuron 75, 786–798. doi:10.1016/j.neuron.2012.06.033

Jimenez-Guri, E., Udina, F., Colas, J.-F., Sharpe, J., Padrón-Barthe, L., Torres, M., Pujades, C., 2010. Clonal analysis in mice underlines the importance of rhombomeric boundaries in cell movement restriction during hindbrain segmentation. PLoS ONE 5, e10112. doi:10.1371/journal.pone.0010112

Kidwell, C.U., Su, C.-Y., Hibi, M., Moens, C.B., 2018. Multiple zebrafish atoh1 genes specify a diversity of neuronal types in the zebrafish cerebellum. Developmental Biology 438, 44–56. doi:10.1016/j.ydbio.2018.03.004

Kiecker, C., Lumsden, A., 2005. Compartments and their boundaries in vertebrate brain development. Nature Reviews Neuroscience 6, 553–564. doi:10.1038/nrn1702

Kimura, Y., Hisano, Y., Kawahara, A., Higashijima, S.-I., 2014. Efficient generation of knock-in transgenic zebrafish carrying reporter/driver genes by CRISPR/Cas9-mediated genome engineering. Sci. Rep. 4, 6545. doi:10.1038/srep06545

Letelier, J., Terriente, J., Belzunce, I., Voltes, A., Undurraga, C.A., Polvillo, R., Devos, L., Tena, J.J., Maeso, I., Rétaux, S., Gómez-Skarmeta, J.L., Martínez-Morales, J.R., Pujades, C., 2018. Evolutionary emergence of the rac3b/rfng/sgca regulatory cluster refined mechanisms for hindbrain boundaries formation. Proc. Natl. Acad. Sci. U.S.A. 115, E3731–E3740. doi:10.1073/pnas.1719885115

Llorca, A., Ciceri, G., Beattie, R., Wong, F.K., Diana, G., Serafeimidou-Pouliou, E., Fernández-Otero, M., Streicher, C., Arnold, S.J., Meyer, M., Hippenmeyer, S., Maravall, M., Marin, O., 2019. A stochastic framework of neurogenesis underlies the assembly of neocortical cytoarchitecture. Elife 8. doi:10.7554/eLife.51381

Louvi, A., Artavanis-Tsakonas, S., 2006. Notch signalling in vertebrate neural development. Nature Reviews Neuroscience 7, 93–102. doi:10.1038/nrn1847

Lowery, L.A., Sive, H., 2009. Totally tubular: the mystery behind function and origin of the brain ventricular system. Bioessays 31, 446–458. doi:10.1002/bies.200800207

Lyons, D.A., Guy, A.T., Clarke, J.D.W., 2003. Monitoring neural progenitor fate through multiple rounds of division in an intact vertebrate brain. Development 130, 3427–3436. doi:10.1242/dev.00569

McDole, K., Guignard, L., Amat, F., Berger, A., Malandain, G., Royer, L.A., Turaga, S.C., Branson, K., Keller, P.J., 2018. In Toto Imaging and Reconstruction of Post-Implantation Mouse Development at the Single-Cell Level. Cell 175, 859–876.e33. doi:10.1016/j.cell.2018.09.031

Nikolaou, N., Watanabe-Asaka, T., Gerety, S., Distel, M., Köster, R.W., Wilkinson, D.G., 2009. Lunatic fringe promotes the lateral inhibition of neurogenesis. Development 136, 2523–2533. doi:10.1242/dev.034736

Park, H.C., Kim, C.H., Bae, Y.K., Yeo, S.Y., Kim, S.H., Hong, S.K., Shin, J., Yoo, K.W., Hibi, M., Hirano, T., Miki, N., Chitnis, A.B., Huh, T.L., 2000. Analysis of upstream elements in the HuC promoter leads to the establishment of transgenic zebrafish with fluorescent neurons. Developmental Biology 227, 279–293. doi:10.1006/dbio.2000.9898

Park, S.-H., Yeo, S.-Y., Yoo, K.-W., Hong, S.-K., Lee, S., Rhee, M., Chitnis, A.B., Kim, C.-H., 2003. Zath3, a neural basic helix-loop-helix gene, regulates early neurogenesis in the zebrafish. BIOCHEMICAL AND BIOPHYSICAL RESEARCH COMMUNICATIONS 308, 184–190. doi:10.1016/S0006-291X(03)01353-6

Peretz, Y., Eren, N., Kohl, A., Hen, G., Yaniv, K., Weisinger, K., Cinnamon, Y., Sela-Donenfeld, D., 2016. A new role of hindbrain boundaries as pools of neural stem/progenitor cells regulated by Sox2. BMC Biol. 14, 57. doi:10.1186/s12915-016-0277-y

Pujades, C., 2020. The multiple functions of hindbrain boundary cells: Tinkering boundaries? Seminars in Cell and Developmental Biology 107, 179–189. doi:10.1016/j.semcdb.2020.05.002

Riley, B.B., Chiang, M.-Y., Storch, E.M., Heck, R., Buckles, G.R., Lekven, A.C., 2004. Rhombomere boundaries are Wnt signaling centers that regulate metameric patterning in the zebrafish hindbrain. Dev. Dyn. 231, 278–291. doi:10.1002/dvdy.20133

Schlager, S., 2017. Morpho and Rvcg – Shape Analysis in R: R-Packages for Geometric Morphometrics, Shape Analysis and Surface Manipulations, in: Statistical Shape and Deformation Analysis. Academic Press, pp. 217–256. doi:10.1016/B978-0-12-810493-4.00011-0

Shimojo, H., Ohtsuka, T., Kageyama, R., 2008. Oscillations in notch signaling regulate maintenance of neural progenitors. Neuron 58, 52–64. doi:10.1016/j.neuron.2008.02.014

Sueda, R., Kageyama, R., 2019. Regulation of active and quiescent somatic stem cells by Notch signaling. Develop. Growth Differ. 128, 689–66. doi:10.1111/dgd.12626

Symonds, A.C., Buckley, C.E., Williams, C.A., Clarke, J.D.W., 2020. Coordinated assembly and release of adhesions builds apical junctional belts during de novo polarisation of an epithelial tube. Development 147. doi:10.1242/dev.191494

Taberner L, Bañón A, Alsina B. 2020. Sensory Neuroblast Quiescence Depends on Vascular Cytoneme Contacts and Sensory Neuronal Differentiation Requires Initiation of Blood Flow. Cell Rep. 2020 Jul 14;32(2):107903. doi: 10.1016/j.celrep.2020.107903.

Terriente, J., Gerety, S.S., Watanabe-Asaka, T., Gonzalez-Quevedo, R., Wilkinson, D.G., 2012. Signalling from hindbrain boundaries regulates neuronal clustering that patterns neurogenesis. Development 139, 2978–2987. doi:10.1242/dev.080135

Than-Trong, E., Kiani, B., Dray, N., Ortica, S., Simons, B., Rulands, S., Alunni, A., Bally-Cuif, L., 2020. Lineage hierarchies and stochasticity ensure the long-term maintenance of adult neural stem cells. Sci Adv 6, eaaz5424. doi:10.1126/sciadv.aaz5424

Thisse, C., Thisse, B., 2008. High-resolution in situ hybridization to whole-mount zebrafish embryos. Nature Protocols 3, 59–69. doi:10.1038/nprot.2007.514

Trevarrow B, Marks DL, Kimmel CB. 1990. Organization of hindbrain segments in the zebrafish embryo. Neuron. 1990 May;4(5):669-79. doi: 10.1016/0896-6273(90)90194-k

Voltes, A., Hevia, C.F., Engel-Pizcueta, C., Dingare, C., Calzolari, S., Terriente, J., Norden, C., Lecaudey, V., Pujades, C., 2019. Yap/Taz-TEAD activity links mechanical cues to progenitor cell behavior during zebrafish hindbrain segmentation. Development 146. doi:10.1242/dev.176735

Wan, Y., Wei, Z., Looger, L.L., Koyama, M., Druckmann, S., Keller, P.J., 2019. Single-Cell Reconstruction of Emerging Population Activity in an Entire Developing Circuit. Cell 179, 355–372.e23. doi:10.1016/j.cell.2019.08.039

Wolff, C., Tinevez, J.-Y., Pietzsch, T., Stamataki, E., Harich, B., Guignard, L., Preibisch, S., Shorte, S., Keller, P.J., Tomancak, P., Pavlopoulos, A., 2018. Multi-view light-sheet imaging and tracking with the MaMuT software reveals the cell lineage of a direct developing arthropod limb. Elife 7, 375. doi:10.7554/eLife.34410

Zechner, C., Nerli, E., Norden, C., 2020. Stochasticity and determinism in cell fate decisions. Development 147, dev181495. doi:10.1242/dev.181495

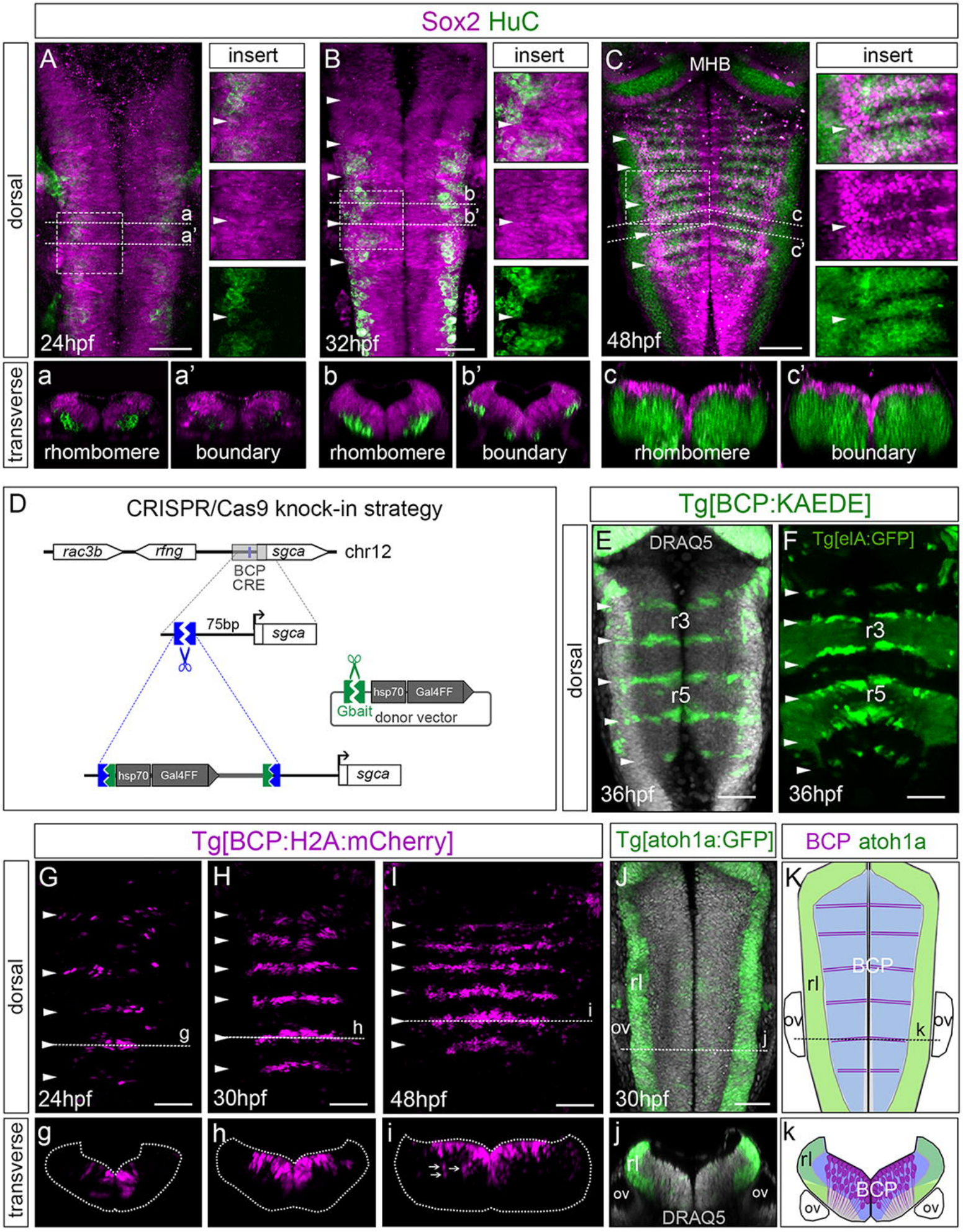
Sox2 HuC
dorsal
transverse
A
insert
a
a'
24hpf
B
insert
b
b'
32hpf
C
MHB
insert
c
c'
48hpf
a
rhombomere
a'
boundary
b
rhombomere
b'
boundary
c
rhombomere
c'
boundary
D
CRISPR/Cas9 knock-in strategy
rac3b
rfng
sgca
chr12
BCP
CRE
75bp
sgca
hsp70
Gal4FF
Gbait
donor vector
hsp70
Gal4FF
sgca
Tg[BCP:KAEDE]
dorsal
E
DRAQ5
r3
r5
36hpf
F
Tg[elA:GFP]
r3
r5
36hpf
Tg[BCP:H2A:mCherry]
Tg[atoh1a:GFP]
BCP atoh1a
dorsal
transverse
G
g
24hpf
H
h
30hpf
I
i
48hpf
J
rl
ov
j
30hpf
K
BCP
rl
ov
k
ov
g
h
i
j
rl
ov
ov
DRAQ5
k
rl
BCP
ov
ov

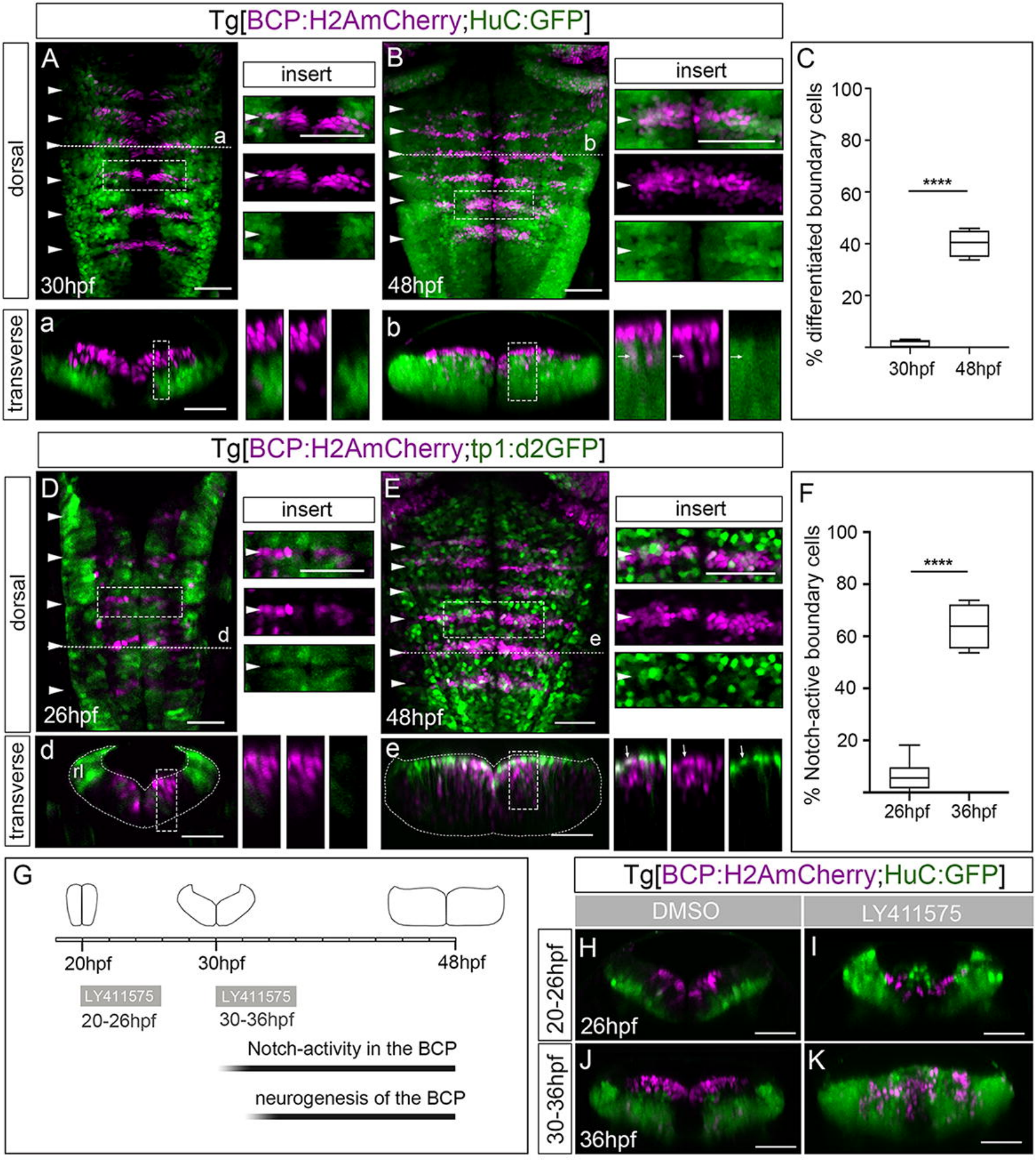
Tg[BCP:H2AmCherry;HuC:GFP]
dorsal
transverse
A
insert
a
30hpf
B
insert
b
48hpf
C
% differentiated boundary cells
100
80
60
40
20
****
30hpf
48hpf
Tg[BCP:H2AmCherry;tp1:d2GFP]
D
insert
d
26hpf
E
insert
e
48hpf
rl
F
% Notch-active boundary cells
100
80
60
40
20
****
26hpf
36hpf
G
20hpf
30hpf
48hpf
LY411575
20-26hpf
LY411575
30-36hpf
Notch-activity in the BCP
neurogenesis of the BCP
Tg[BCP:H2AmCherry;HuC:GFP]
DMSO
LY411575
20-26hpf
30-36hpf
H
26hpf
I
J
36hpf
K

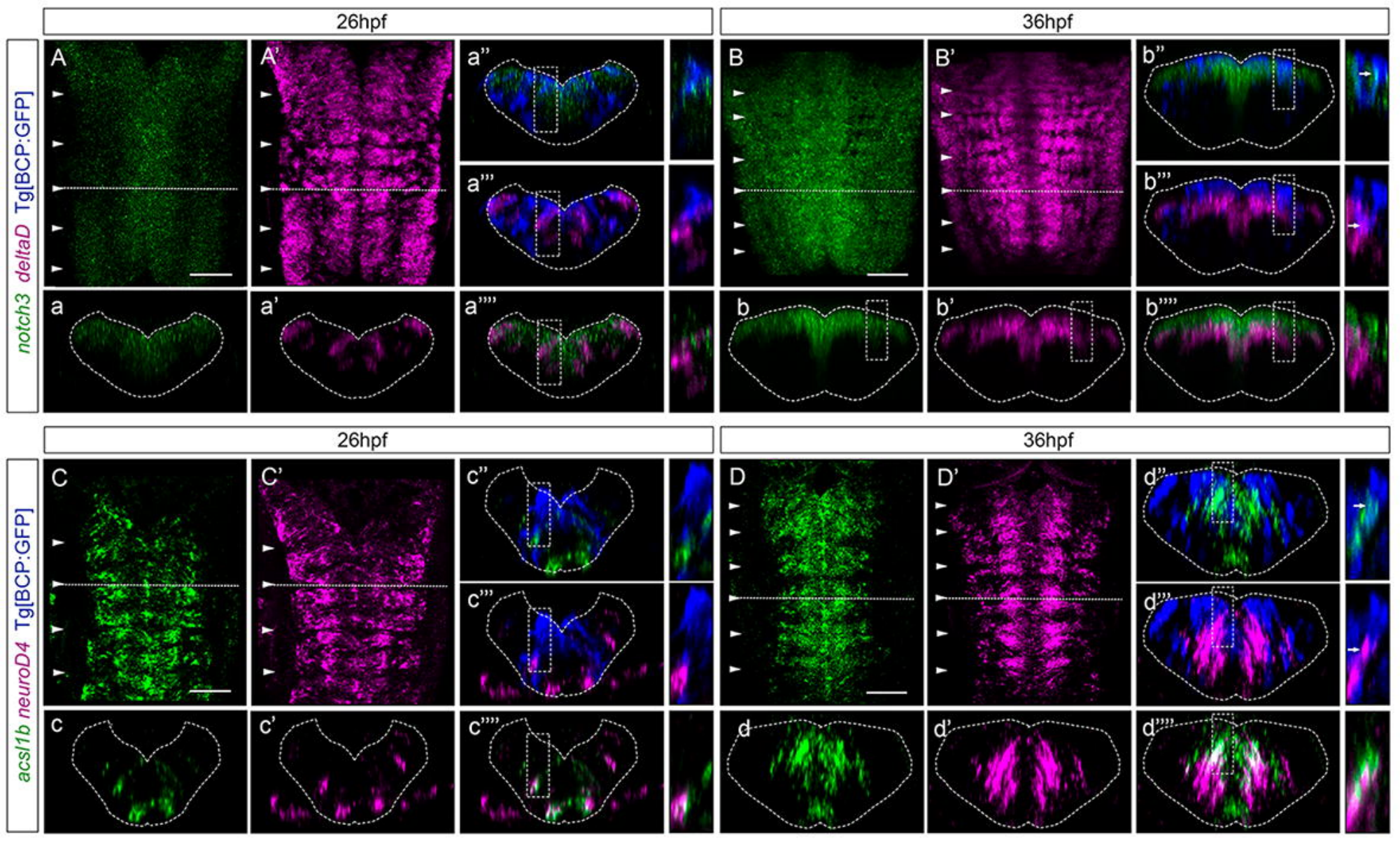
26hpf
36hpf
notch3 deltaD Tg[BCP:GFP]
A
A'
a''
a'''
a
a'
a''''
B
B'
b''
b'''
b
b'
b''''
26hpf
36hpf
acsl1b neuroD4 Tg[BCP:GFP]
C
C'
c''
c'''
c
c'
c''''
D
D'
d''
d'''
d
d'
d''''

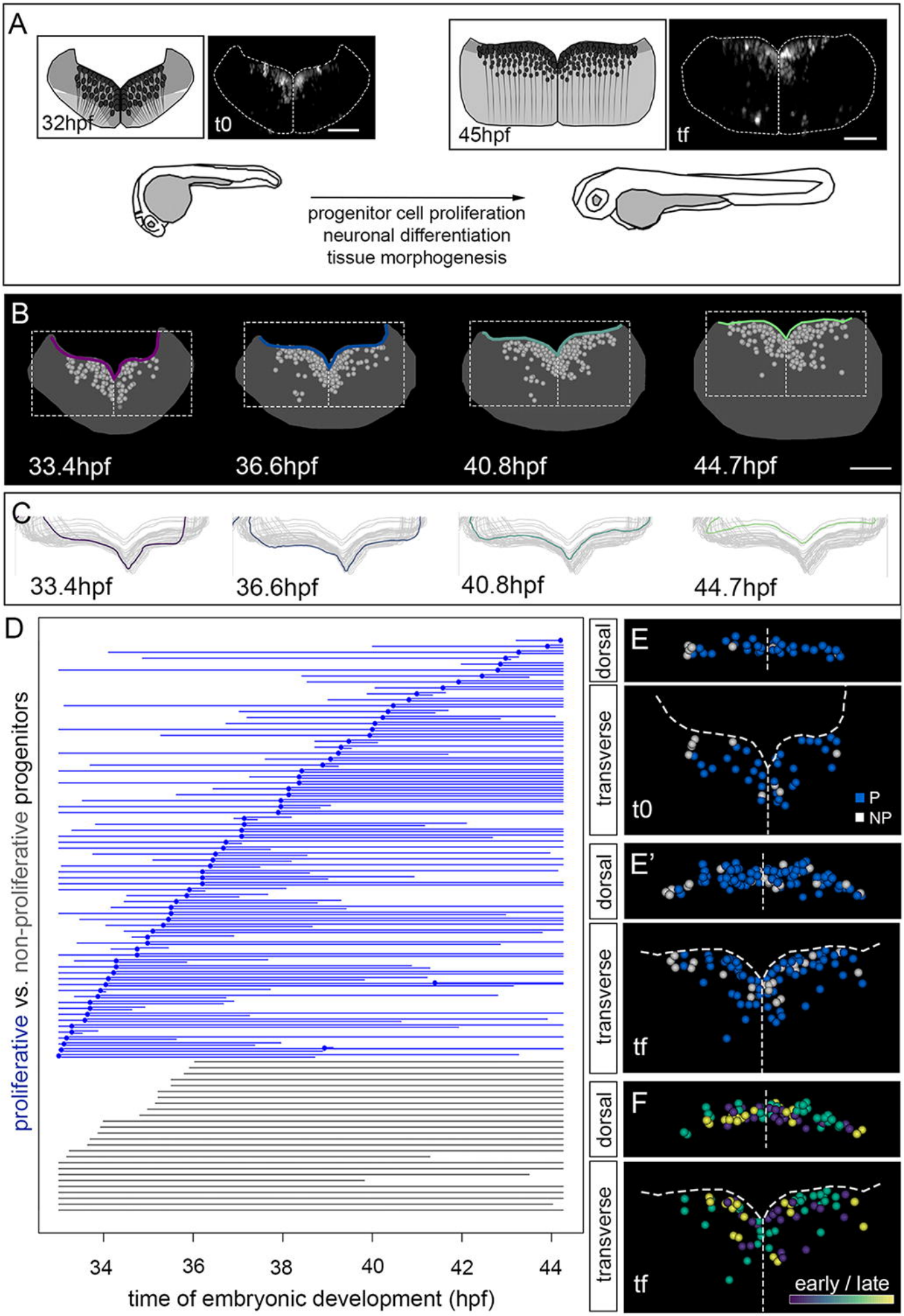
A
32hpf
t0
45hpf
tf
progenitor cell proliferation
neuronal differentiation
tissue morphogenesis
B
33.4hpf
36.6hpf
40.8hpf
44.7hpf
C
33.4hpf
36.6hpf
40.8hpf
44.7hpf
D
proliferative vs. non-proliferative progenitors
34
36
38
40
42
44
time of embryonic development (hpf)
dorsal
E
transverse
t0
P
NP
dorsal
E'
transverse
tf
dorsal
F
transverse
tf
early / late

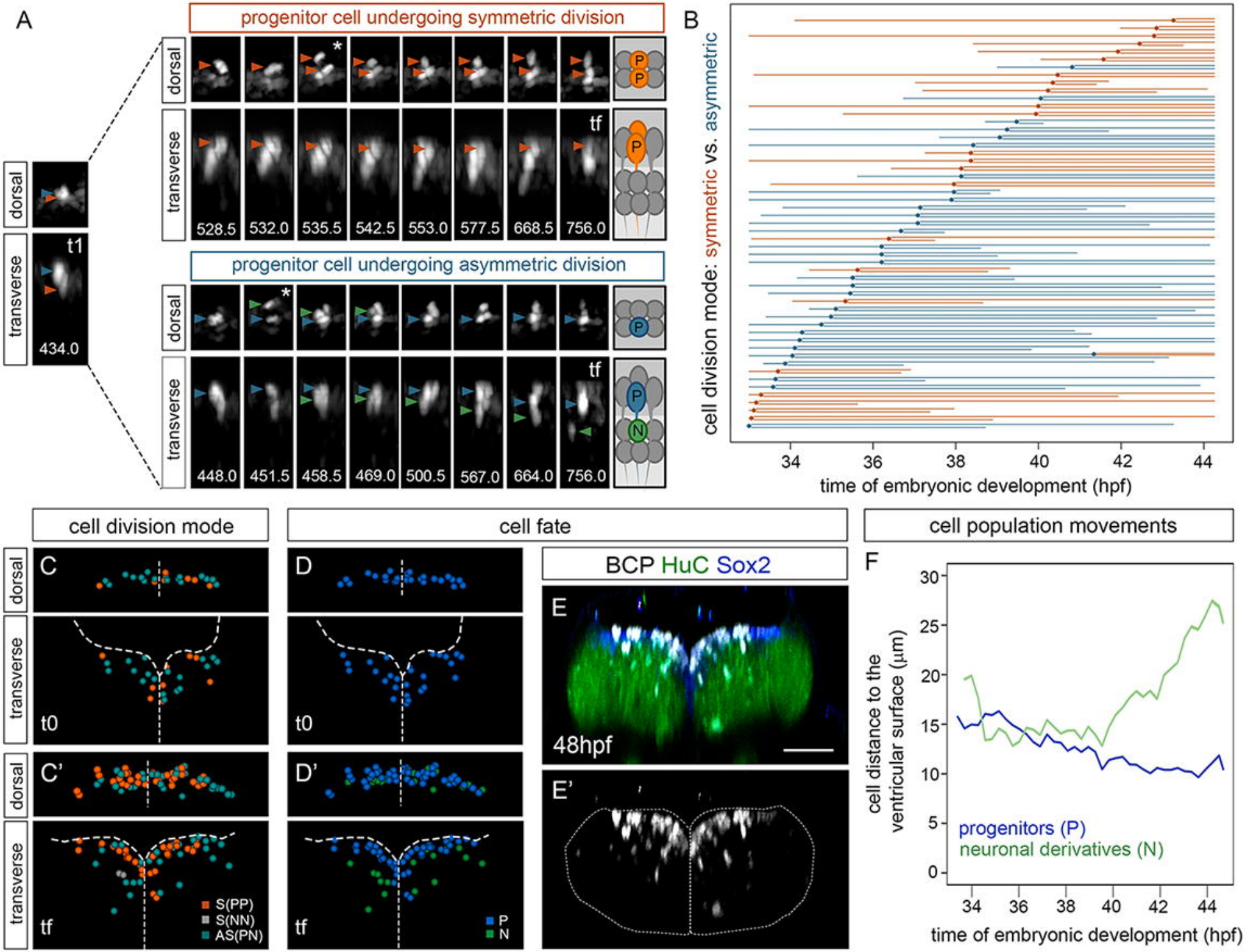
A
progenitor cell undergoing symmetric division
dorsal
transverse
t1
434.0
528.5
532.0
535.5
542.5
553.0
577.5
668.5
756.0
tf
P
progenitor cell undergoing asymmetric division
448.0
451.5
458.5
469.0
500.5
567.0
664.0
756.0
N
B
cell division mode: symmetric vs. asymmetric
time of embryonic development (hpf)
34
36
38
40
42
44
cell division mode
cell fate
cell population movements
C
C'
D
D'
t0
tf
S(PP)
S(NN)
AS(PN)
BCP HuC Sox2
E
E'
48hpf
F
cell distance to the ventricular surface (µm)
progenitors (P)
neuronal derivatives (N)

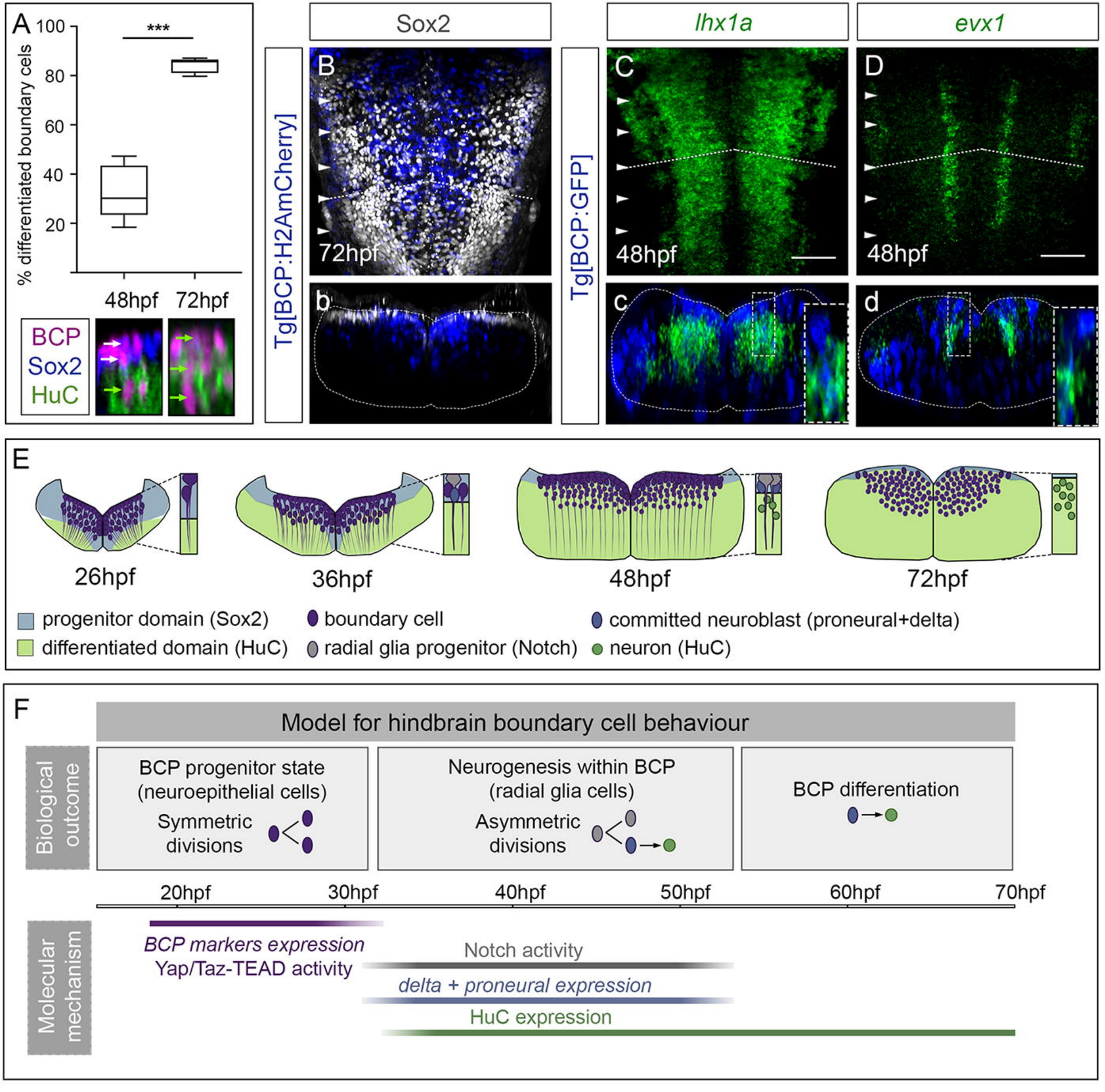
A
% differentiated boundary cels
100
80
60
40
20
***
48hpf
72hpf
BCP
Sox2
HuC
Sox2
Tg[BCP:H2AmCherry]
B
72hpf
b
lhx1a
evx1
Tg[BCP:GFP]
C
48hpf
D
48hpf
c
d
E
26hpf
36hpf
48hpf
72hpf
progenitor domain (Sox2)
differentiated domain (HuC)
boundary cell
radial glia progenitor (Notch)
committed neuroblast (proneural+delta)
neuron (HuC)
F
Model for hindbrain boundary cell behaviour
Biological outcome
BCP progenitor state (neuroepithelial cells)
Symmetric divisions
Neurogenesis within BCP (radial glia cells)
Asymmetric divisions
BCP differentiation
20hpf
30hpf
40hpf
50hpf
60hpf
70hpf
Molecular mechanism
BCP markers expression
Yap/Taz-TEAD activity
Notch activity
delta + proneural expression
HuC expression